ORIGINAL ARTICLE

lajss.org© Latin American Journal of Solids and Structures

www.lajss.org

Response of combined formwork construction with precast concrete laminated slab and steel truss to flexural loading

Tao Liang[a], Mei Feng[b], Yanhui Wei[c,d], Hanming Zhang[c,d], Jing Chen[c,d]*

[a] Institute of Engineering Investigation and Design, Guizhou University, Guiyang 550025, China. Email: 13902572@qq.com
[b] Guizhou Institute of Technology, Guiyang 550003, China. Email: 28292453@qq.com
[c] Research Center of Space Structures, Guizhou University, Guiyang 550025, China. Email: zhm_gzu@163.com, yhwei@gzu.edu.cn, *jchen23@gzu.edu.cn
[d] Key Laboratory of Green Building and Intelligent Construction of Guizhou Province, Guiyang 550025, China.

* Corresponding author

https://doi.org/10.1590/1679-7825/e8851

Abstract

This paper presents a precast concrete composite slab-steel truss formwork system incorporating demountable joints to achieve composite behavior between the upper slab and the lower truss, thereby facilitating truss reuse. The system enables shoring-free construction for medium to long spans(3.0m~6.0m), enhancing construction efficiency and reducing material consumption. To assess its performance under realistic conditions, three full-scale specimens were subjected to vertical static bending tests involving a loading-unloading procedure. A finite-element model was developed and calibrated against experimental results, followed by a parametric analysis. The system demonstrated excellent flexural performance with minimal residual deformations after unloading, indicating high recoverability and reliable reusability. Parametric studies reveal that increasing slab thickness primarily enhances the slab's behavior with negligible influence on the global structural response, whereas truss height and member cross-sections predominantly govern overall stiffness and load-bearing capacity. Based on experimental and numerical findings, simplified design equations for strength and deflection are proposed to support design optimization and practical implementation.

Keywords

Precast composite slab; Steel truss; Demountable joint; Static bending test; Finite element analysis; Parametric study; Simplified design method

Graphical Abstract

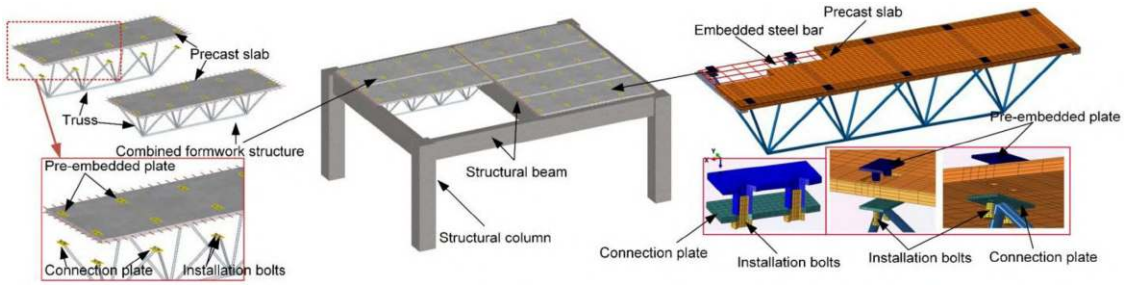

Received September 24, 2025. In revised form December 14, 2025. Accepted January 04, 2026. Available online January 08, 2026.
https://doi.org/10.1590/1679-7825/e8851

Latin American Journal of Solids and Structures. ISSN 1679-7825. Copyright © 2026. This is an Open Access article distributed under the terms of the Creative Commons Attribution license, which permits unrestricted use, distribution, and reproduction in any medium, provided the original work is properly cited.

1 INTRODUCTION

The composite slab is composed of a precast bottom slab and an upper cast-in-place reinforced-concrete layer, in which the precast bottom slab simultaneously serves as a load-bearing member and as permanent formwork, while the upper cast-in-place layer is used to ensure the slab's overall working performance (PCI Design Handbook; Nie et al. 2006; Li et al. 2012). Enhancing the flexural capacity and stiffness of such slabs is essential for improving their adaptability and expanding their engineering applications.

The existing research primarily focuses on improving the performance of composite slabs from material innovations and structural improvements. Bayasi et al. (2001) demonstrated that corrugated HPFRC panels, used in place of profiled steel decks, achieve satisfactory composite flexural performance with the concrete topping, supporting their use as a viable alternative to conventional profiled-steel composite slabs. Abas et al. (2013) and Yu et al. (2024) conducted static loading tests on fiber-reinforced concrete composite slabs to evaluate the influence of fiber content on cracking behavior in the negative bending region and interlayer slip. Researchers (Lu et al. 2022; Lu et al. 2022; Jing et al. 2020; Zhang et al. 2022a, b; Mohamad et. al. 2016; Wang et al. 2024) replaced natural aggregates with recycled aggregate concrete (RAC) and conducted bending tests to reveal the failure mechanisms of recycled concrete composite slabs under different parameters. Researchers incorporated lightweight aggregates into the concrete of composite slabs, achieving a reduced self-weight without compromising flexural capacity or crack resistance (Deng et al. 2023; Sun et al. 2023; Mohammed 2010).

Researchers have improved composite slab systems by developing sandwich slabs with various core infill materials, achieving lower self-weight than conventional concrete slabs of the same thickness. Adjusting the core-layer thickness enables span-specific design while also offering thermal and acoustic advantages. Enhanced reinforcement connection methods further improve composite action between the core material and concrete, thereby increasing vertical load-bearing capacity (Tomlinson and Fam. 2016; Thanoon et al. 2010; Joseph et al. 2017; Lu et al. 2022). In addition, composite floors composed of prestressed concrete hollow-core units and a cast-in-place concrete topping exhibit enhanced flexural behavior. The prestressing action significantly reduces cracking and improves the initial stiffness of the composite slab. (Baran 2015; Girhammar and Pajari 2008; Araújo et al. 2020; Li et al. 2025). Yong et al. (2018) proposed a steel–concrete composite slab system consisting of a flat steel plate bonded to a concrete slab through perforated shear connectors. Experimental results demonstrated strong composite action between the two materials, leading to favorable overall structural performance.

Notably, existing studies primarily focus on the service performance of composite slabs after formation, with limited attention given to the mechanical behavior during the construction stage, when the topping layer has not yet participated in the structural response. The widely adopted lattice girder slab integrates a steel reinforcement truss within the precast base panel, can improve the stiffness and load-bearing capacity of the precast bottom slab during the construction stage (Yun et al. 2022; Hillebrand et al. 2021; Wieneke et al. 2017; Lee et al. 2024). However, for longer erection spans (3.0~6.0 m), meeting deflection criteria and safety requirements typically necessitates temporary shoring. Under tall formwork, the added bracing raises construction complexity and material consumption, eroding the efficiency gains of the prefabricated scheme.

Based on the above, this paper proposes a novel composite formwork system combining prefabricated concrete composite slabs with steel truss frameworks. As shown in Figure 1, the system in which a precast slab is partially connected to a steel truss, via demountable connectors. The resulting slab–truss composite (Wei et al. 2014; Yin et al. 2017) is seated on beams or walls, providing a stable support framework. The upper precast layer serves as the construction platform for the cast-in-place topping, and the construction detailing (JGJ-1-2014; T/CECS 75-2020) is shown in Figure 2. Once the cast-in-place topping attains its specified strength, the underlying steel truss is dismantled and redeployed, enabling cyclical reuse of materials. The proposed system is intended for use in building floor structures with medium-span slabs (approximately 3–6 m). During the construction stage, it can effectively control the deflection and load-bearing capacity of the precast slab, significantly reducing the need for conventional formwork, accelerating construction progress, and lowering material consumption.

This study performed static flexural loading and unloading tests on three full-scale specimens, acquiring displacement responses at key measurement points to evaluate the stiffness, load-bearing capacity, and residual deformation after unloading, thereby assessing the system's recoverability and its reliability for repeated reuse. Based on ABAQUS, a finite element model was established, calibrated it against the experimental results to clarify the slab–truss load-sharing path, quantify the stiffness contributions, and reveal the mechanisms of internal force redistribution. Furthermore, a sensitivity study of key design parameters is conducted to quantify the influence of the thickness of the composite slab, the height of the truss, and the cross-section of the members on the load-bearing capacity and overall stiffness, identifying the controlling parameters to provide a basis for the selection of span and structural configuration. Finally, a simplified calculation method for load-bearing capacity and deflection oriented toward engineering application is proposed, providing practical technical support for the promotion and application of this system.

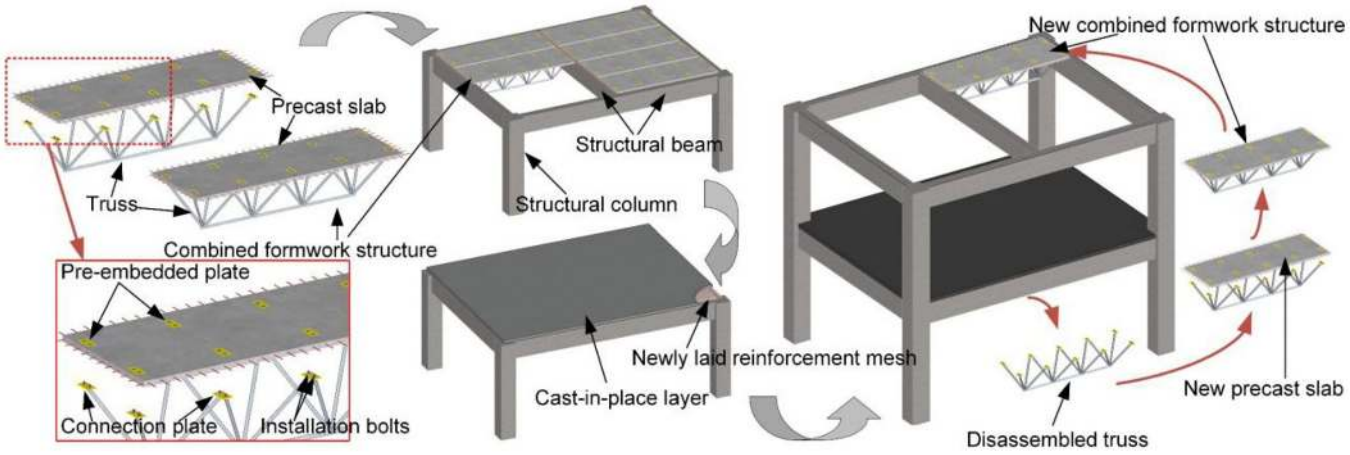

Figure 1 Schematic of combined formwork structure with precast concrete laminated slab and steel truss.

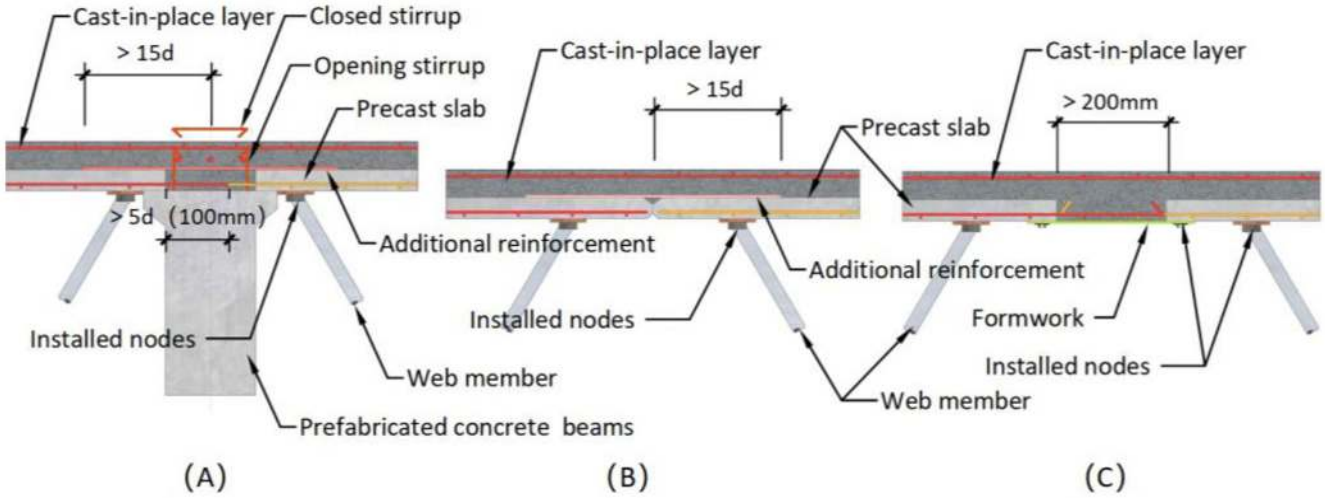

Figure 2 Schematic of assembly joint.

2 Experimental program

2.1 Design and Fabrication of Experimental Models

The experiment utilized full-scale models, with three identical-sized specimens fabricated to ensure the accuracy of the experimental data. Table 1 presents the detailed dimensions, with EM1, EM2, and EM3 referring to the three full-scale specimens incorporating different unloading sequences. The structural configuration is illustrated in Figure 3.

The model design span is 4300 mm (L), the plate width is 1200 mm (B), and the prefabricated concrete plate thickness is 50 mm (H1). The concrete had a characteristic cube compressive strength of 30 MPa, and the reinforcing bars had a yield strength of 400 MPa. Longitudinal bars (ϕ10) were placed at 150 mm spacing, while the constructional reinforcement (ϕ8) was arranged at 200 mm spacing. The precast slabs were fabricated in the laboratory and subsequently cured under ambient conditions for 28 days prior to the loading tests.

The lower steel truss was fabricated using circular hollow sections with an outer diameter of 32 mm and a wall thickness of 3.0 mm, possessing a nominal yield strength of 235 MPa. The truss height was 800 mm (H2). The web members are welded to the lower connection plates, while the upper embedded plate is welded to the coupler and cast in place at the designated position within the precast slab, the joints were welded using continuous single-sided fillet welds with a weld leg size of 4 mm. Both the lower connection plate and the upper embedded plate have dimensions of 150 mm × 100 mm × 10 mm and are made of the same material as the steel truss, characterized by a nominal yield strength of 235 MPa.

At each joint, the upper slab was connected to the lower steel truss using two M20 high-strength bolts of Grade 10.9, the bolts pass through the bolt holes in the lower connection plate and are anchored into the embedded couplers for fixation, forming a complete prefabricated concrete composite slab and steel truss composite formwork system. The node construction is shown in Figure 4.

Table 1 Details of experimental model.

Type	L(mm)	B(mm)	H1(mm)	H2(mm)	Bolt	Concrete grade	reinforced bar grade
EM1 EM2 EM3	4300	1200	50	800	M20	30 Mpa	400 MPa
	Section of truss member			Constructional bar		Longitudinal carrying bar	
	Ø32 X3.0 (235Mpa)			ϕ 8@200mm		ϕ 10@150 mm	

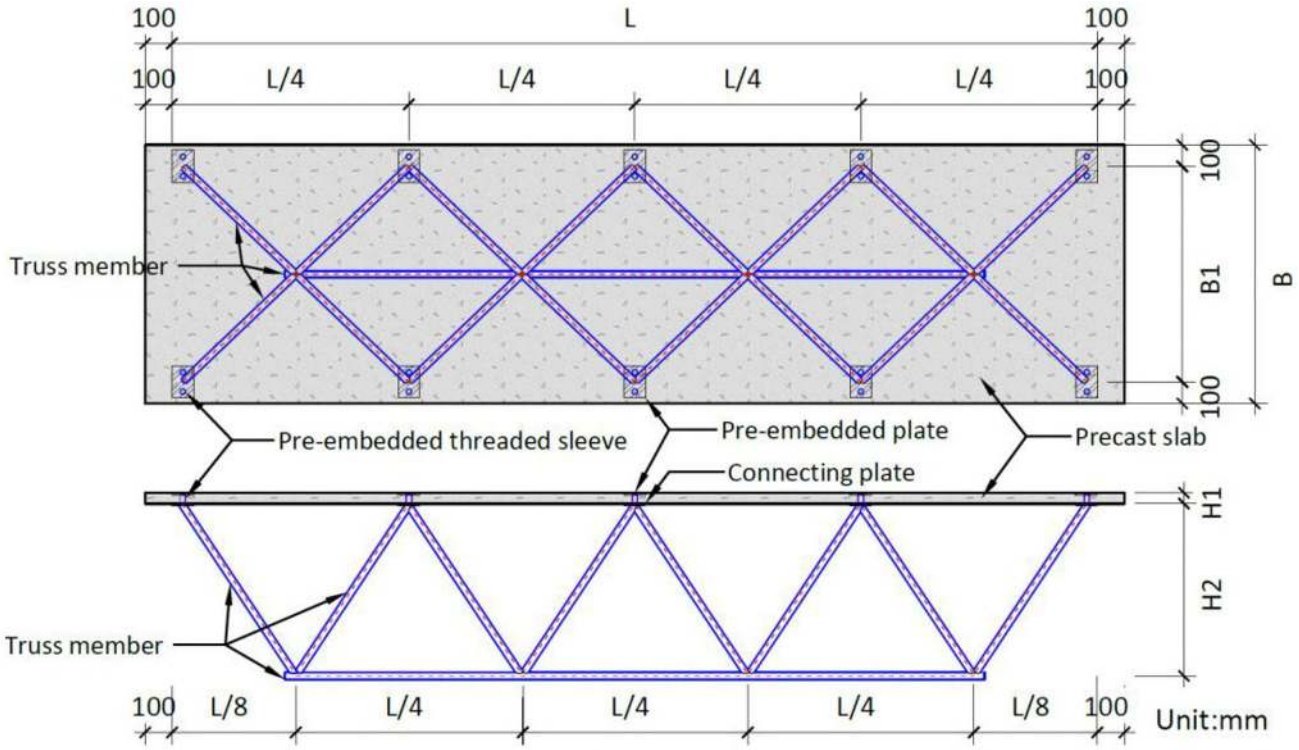

Figure 3 Dimensional drawing of the experimental model.

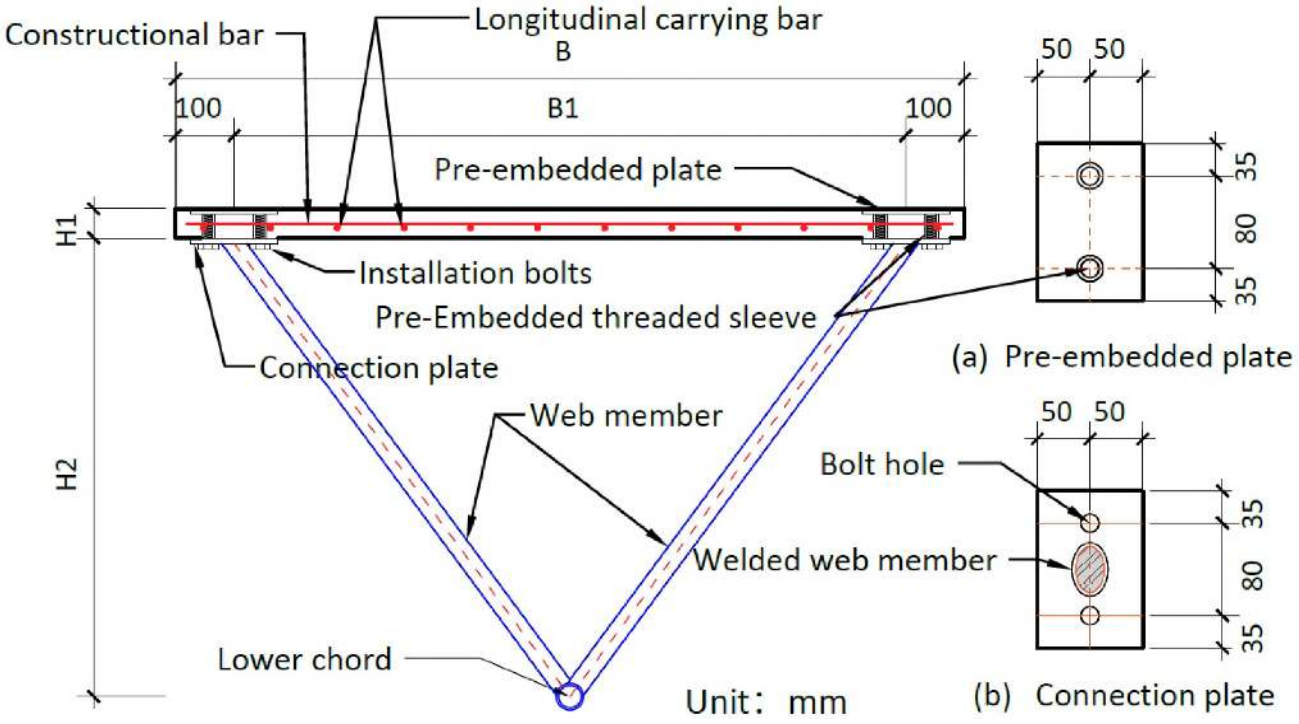

Figure 4 Construction drawing of install node.

As shown in Figure 5, the lower steel truss was built to the specified dimensions, with bolt-holed connection plates (100 × 150 × 10 mm) welded to the ends of all web members. The experimental support system comprised a brick masonry base topped by a reinforced-concrete beam (370 × 200 mm), providing a realistic representation of the in-service support conditions. Set up the formwork and place the reinforcement mesh. Threaded couplers are pre-welded to the embedded steel plates at the predetermined positions, and then fine-aligned using the steel truss for secondary positioning. Once the layout is confirmed, spot-weld the embedded plates to the rebar mesh to keep them from shifting during concreting. After the concrete has been cured to the design strength, the steel truss is bolted to the precast slab to form a single unit. The unit is hoisted onto the supports and positioned, after which the load test is performed.

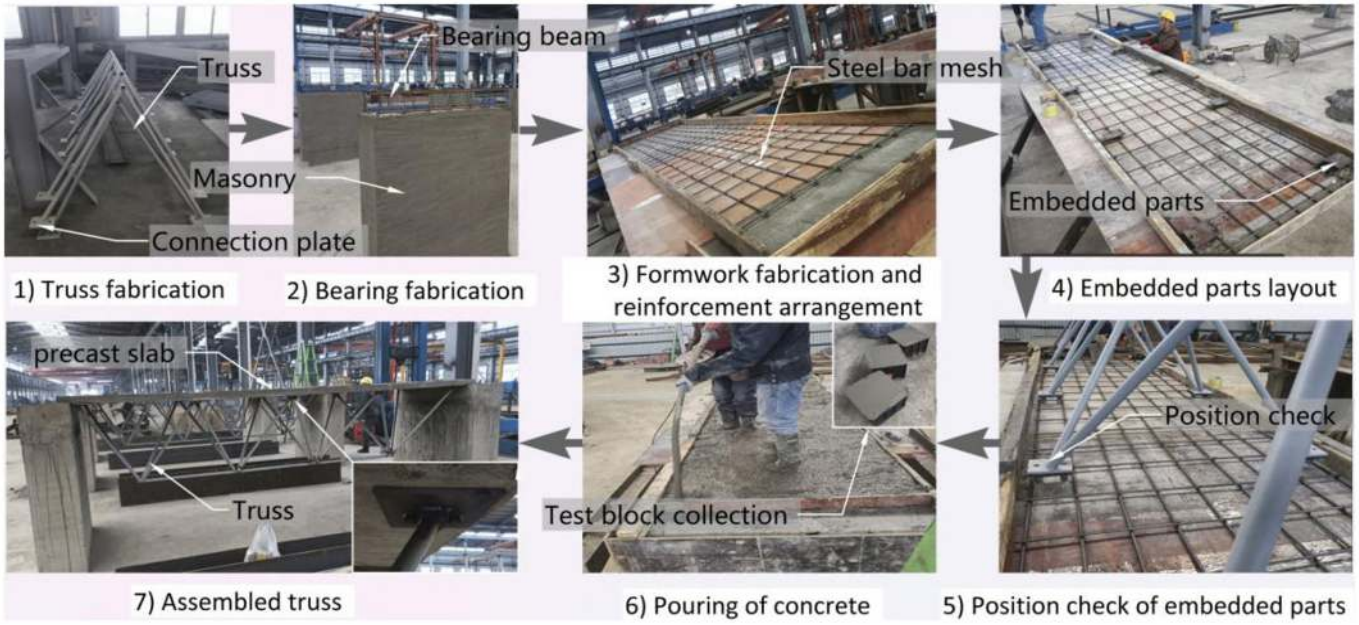

Figure 5 Construction process of the experimental model.

2.2 Measurement and Loading Protocol

The strain and displacement responses of key locations in the test model were monitored under quasi-static incremental loading and unloading. Strain gauges were installed on the prefabricated concrete slab, truss members, and node plates to record the evolution of strain during loading and unloading cycles. Displacement meters were installed on the lower chord of the steel truss to monitor the vertical displacement of the structure. The arrangement and numbering of the measurement points are shown in Figure 6.

The prefabricated concrete composite slab and steel truss combined formwork system, as a self-supporting formwork structure, is used to evaluate the structural behavior in terms of force and deformation during the construction stage. The structure is subjected to the self-weight of a 70 mm thick cast-in-place concrete overlay (1.75 kN/m^2) and construction live load (2.0 kN/m^2). Once the composite layer reaches its design strength, the structure transitions to normal service conditions. To maintain reliability over the full construction period, the system must provide adequate initial stiffness to control early-stage deflection before the topping sets, and demonstrate good recoverability under construction live loads—meaning minimal residual deformation after unloading.

Loading was applied in graded static increments, using sandbags (0.25 kN per piece) and iron blocks (0.20 kN per piece) as load units. Each load increment was 2.0 kN/m^2 (about 10.8 kN per specimen for each step). After a 25 minute stabilization period, the data were recorded and the next level was applied, until loading was terminated at a maximum surface load of 10.0 kN/m^2. All three specimens used the same loading protocol, but their unloading schemes differed: EM1 was unloaded in one step after the final stabilization; EM2 was reduced to 50%, held for 25 minutes, and then fully unloaded; EM3 was reduced to 20%, held for 25 minutes, and then fully unloaded. The detailed loading and unloading procedures are given in Table 2, and photographs of the test setup are shown in Figure 7.

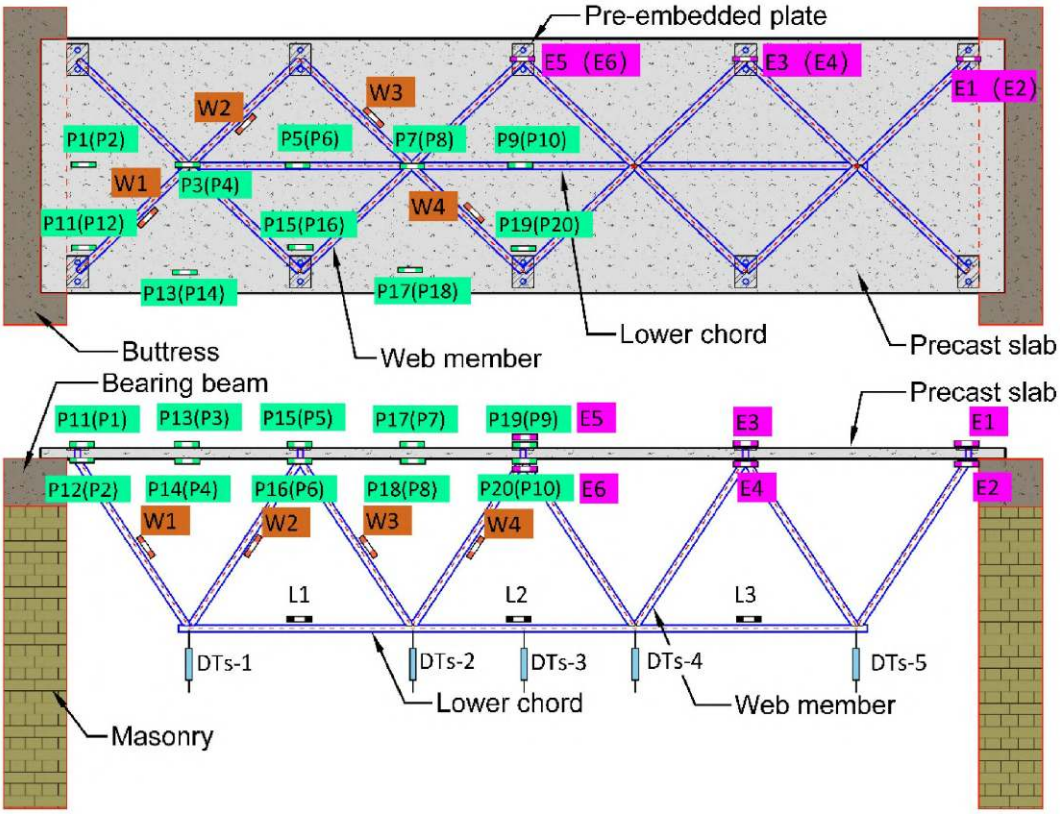

Figure 6 Layout and numbering illustration of strain gauge and displacement meter.

Table 2 Table of loading steps for experimental models.

Type	Preloading steps(kN/m²)		Loading steps(kN/m²)					Unloading steps(kN/m²)	
	Step1	Step2	Step3	Step4	Step5	Step6	Step7	Step8	Step9
EM1								0	-
EM2	2.0	0	2.0	4.0	6.0	8.0	10.0	5.0	0
EM3								8.0	0

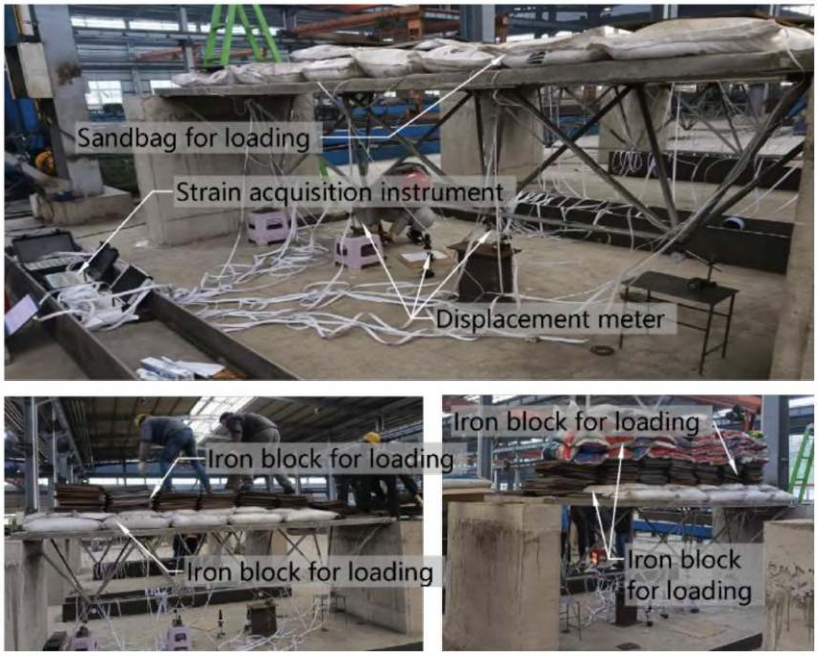

Figure 7 Real scene image of experimental model loading.

3 Test results and discussion

3.1 Load–vertical deflection curve

Figure 8 presents the vertical displacement variations at each displacement monitoring point for the three specimens under stepwise loading. The structure primarily undergoes bending deformation, with a nearly symmetric concave deflection distribution. The maximum displacement occurs at the mid-span (DTs-3), while the displacements at the side spans (DTs-1, DTs-5) are relatively smaller. Following a preload of 2.0 kN/m^2 and full unloading, a small residual deflection of up to 0.34 mm was observed due to slight sliding at the connection interface. As the load increased, the displacements at all measurement points increased proportionally, with no abrupt changes observed. When the fifth-level load (10 kN/m^2) is applied, the mid-span deflections of the three specimens are 3.67 mm, 3.79 mm, and 3.75 mm, respectively, which is approximately 1/1050 of the calculated span. After full unloading, no cracks were observed in the precast slab. The maximum residual deformation was 0.96 mm, corresponding to a residual ratio of 25.6%. The above results indicate that, within the loading range of this test, the structural response is predominantly elastic, but some irrecoverable deformation is present; under a load of 10 kN/m^2, the structure still possesses sufficient load-bearing capacity and good recoverability.

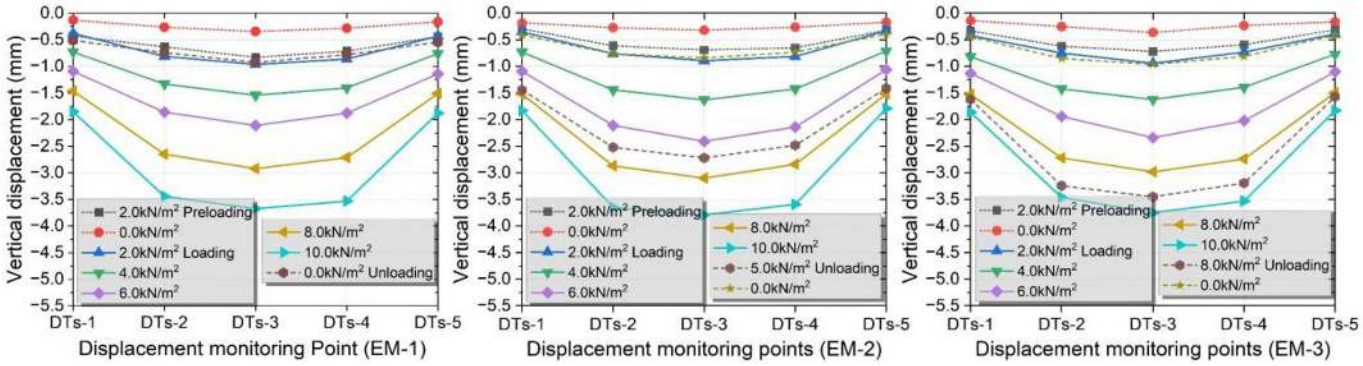

Figure 8 Vertical displacement curve of monitoring points at different loading step.

3.2 Strain variation

Figure 9 shows the strain evolution of the concrete slab measurement points for the three specimens under the three loading conditions as the loading steps progress. All three specimens show the same strain-development pattern, with only minor residual strain remaining after full unloading. In the composite structural system, the upper concrete slab, acting as the upper chord member, experiences more stringent constraints at the support regions. Due to the effects of slip and deformation coordination at the connection interface, the strain in the mid-span regions (P7, P8, P17, P18) is generally less than that in the support regions (P3, P4, P13, P14). Among the slab's measurement points, the peak compressive strain occurred at P13 (153.23), while the peak tensile strain was recorded at P14 (102.43). Here, με denotes microstrain (10^{-6}). Strain redistribution was observed at loading step 7. The local stiffness of the connected nodes and the concentrated constraint action lead to significant asymmetric strain in the concrete slabs near the node plates and the transverse connections of the node plates. This strain may even manifest as the same sign (e.g., P9 and P10, P19 and P20). At mid-span near the connection, the top-surface gauges (P3, P7, P13, P17) mainly recorded compression, whereas the bottom-surface gauges (P4, P8, P14, P18) mainly recorded tension. The compressive strains were slightly larger in magnitude than the tensile strains. The overall behavior of the system is primarily bending-dominated, but the influence of connection constraints and interface slip results in a strain distribution pattern that differs from that of traditional pure bending members.

The strain development curves of the monitoring points on the truss chord (L1, L2, L3) and the embedded plate, as shown in Figures 10 and 11, demonstrate that the truss chord (L1, L2, L3) remains under tension throughout the loading process, with the strain increasing approximately linearly with the loading progression. The peak strain at the mid-span monitoring points is approximately 700 . The strain values in the web members near the supports (W-1, W-2) are approximately 350, while those in the middle span (W-3, W-4) are approximately 100 . The strain distribution in the web members alternates between tension and compression from the supports to the mid-span. The upper and lower node plates (E-1, E-2) near the supports exhibit tensile strain, with the strain in the lower node plate (E-2) being significantly greater than that in the upper node plate (E-1). Because the second-row embedded plates (E-3, E-4) link to one tensile and one compressive web member, the lower gusset plate (E-4) experiences a marked rise in tensile strain (380), while the upper plate (E-3) carries a modest tensile strain (50). By contrast, strains in the mid-span gusset plates remain small.

After unloading, residual strains are observed at the monitoring points of the truss members and embedded plates, indicating minor irreversible deformation in the system, such as micro-slip at the connection interfaces or localized micro-yielding. However, the overall response remains predominantly elastic.

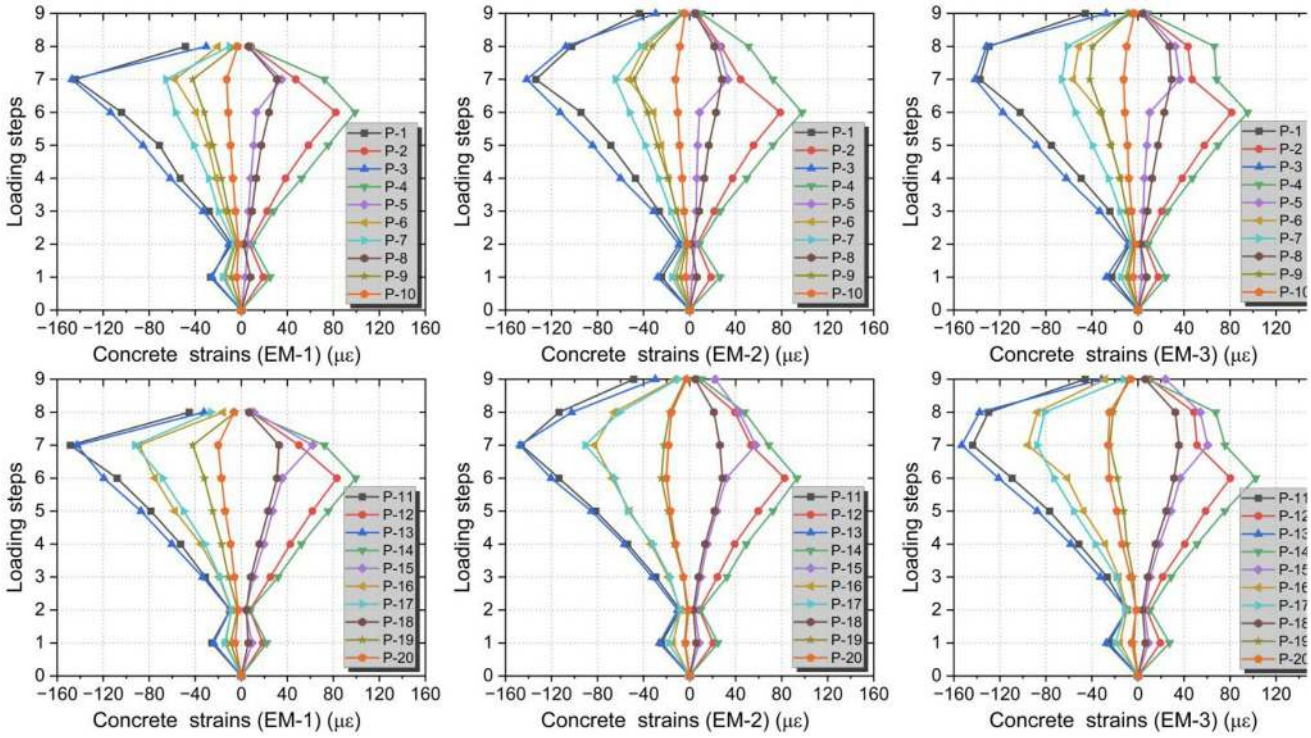

Figure 9 Concrete strains of monitoring points at different loading step.

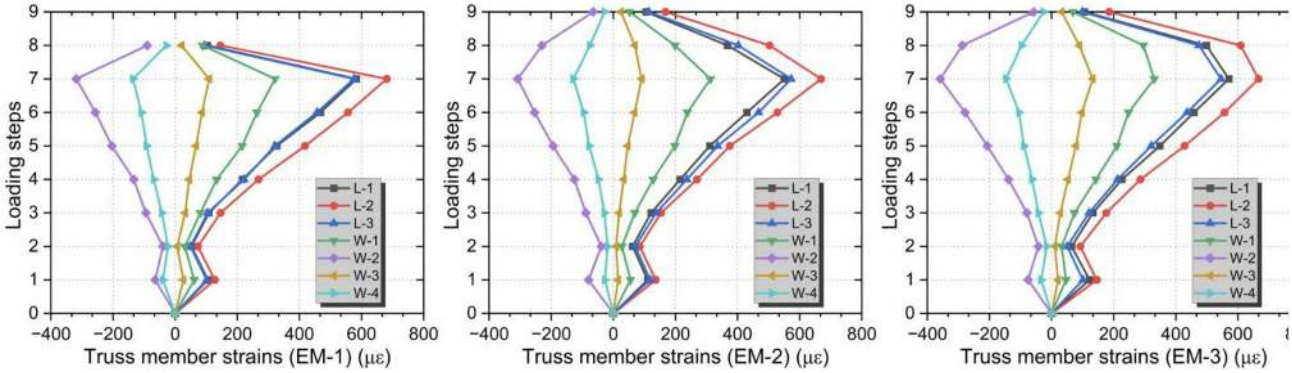

Figure 10 Truss member strains of monitoring points at different loading step.

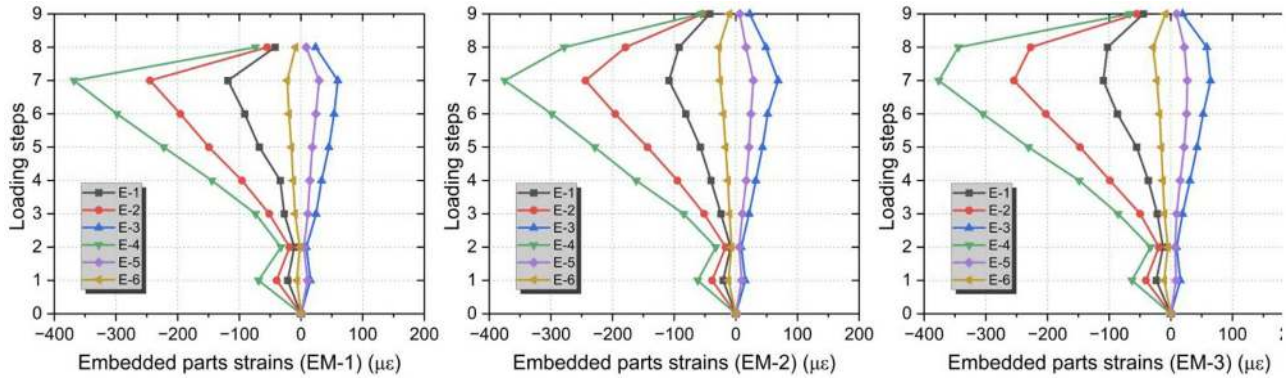

Figure 11 Embedded parts strains of monitoring points at different loading step.

4 Finite element modeling based on ABAQUS

4.1 Material constitutive relation of FE model

A detailed finite element model was developed in ABAQUS based on the experimental specimens. The stress–strain relationship of the steel followed the provisions of the Chinese Code for Design of Concrete Structures (GB50010-2010) and was simplified in the model as a three-segment piecewise linear curve under monotonic loading, neglecting material nonlinearities. In this model, denotes the elastic modulus of the steel, and are the representative yield and ultimate strengths, is the yield strain, marks the onset of strain hardening, is the hardening slope, and is Poisson's ratio. The corresponding parameter values of steel are listed in Table 3, the constitutive relation curves of steel are shown in figure 12-1.

To capture the nonlinear behavior and failure mechanisms of concrete, including damage evolution and crack propagation, the concrete constitutive model was based on the uniaxial tensile and compressive stress–strain relationships specified in the Chinese Code for Design of Concrete Structures (GB50010-2010). Corresponding tensile and compressive damage parameters were incorporated to define the material degradation, enabling the implementation of the Concrete Damaged Plasticity (CDP) model in ABAQUS. Specifically, denotes the concrete elastic modulus, and are the representative uniaxial tensile and compressive strengths, and are the peak tensile and peak compressive strains associated with and , and are the tensile and compressive damage evolution parameters in the CDP formulation, and is Poisson's ratio. The full set of parameter values of concrete is listed in Table 3, the constitutive relation curves of concrete are shown in figure 12-2.

Table 3 Tested material properties of steel and concrete.

Material	E_s(MPa)	$f_{y,r}$(MPa)	ε_y	$f_{st,r}$(MPa)	ε_{uy}	ν_s
Steel parts	2.0X10^5	235	1.05 X10^{-3}	310	1.57 X10^{-2}	0.3
Material	E_c(MPa)	$f_{t,r}$(Mpa)	$\varepsilon_{t,r}$	$f_{c,r}$(MPa)	$\varepsilon_{c,r}$	ν_c
Concrete parts	3.0X10^4	2.01	9.5X10^{-5}	20.1	1.64X10^{-3}	0.2

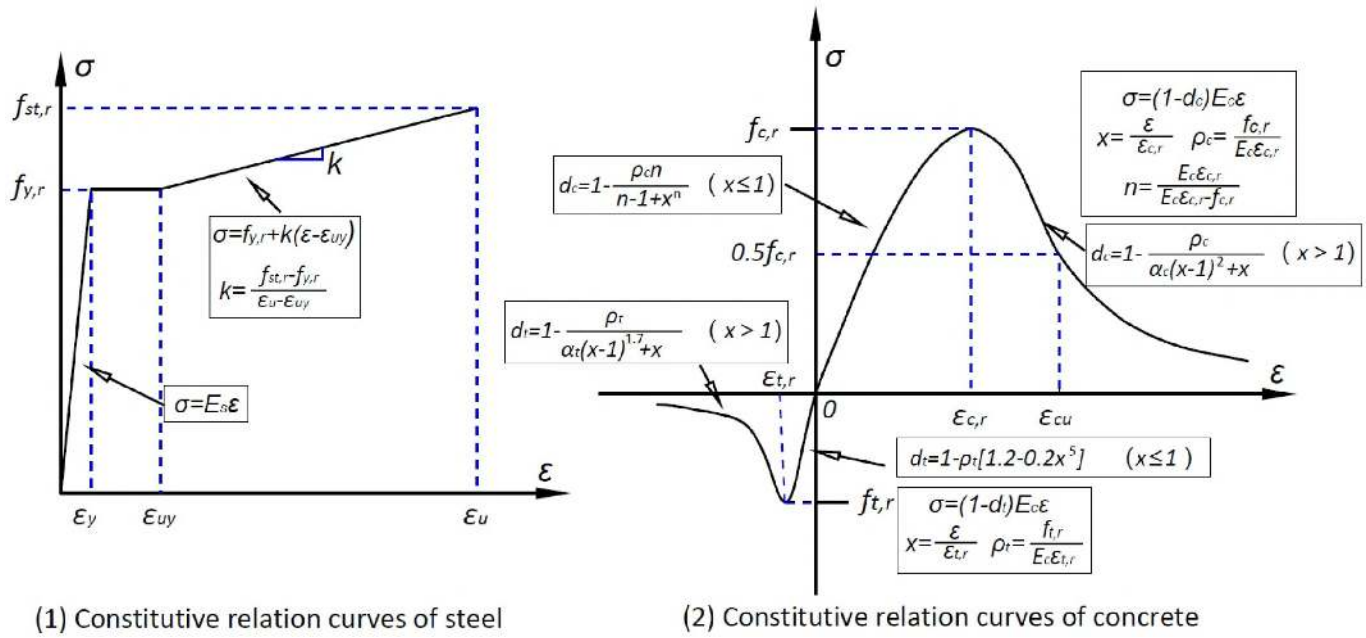

Figure 12 Constitutive relation curves of materials.

4.2 Establishment of the FE model

A finiteelement model was developed based on the dimensions of the test specimens, with the component relationships illustrated in Figure 13. To satisfy the required computational accuracy, different element types were selected to represent the structural members, and a range of mesh densities was employed flexibly throughout the model.

Concrete components were modeled using 3D solid homogeneous elements (C3D8R). Reinforcement bars were represented by embedded 1D truss elements (T3D2), assuming perfect bond. The steel truss members were modeled using beam elements (B31), whereas the connection plates and bolts were modeled using 3D solid elements to capture the detailed load transfer in the detachable joint.

In the finite element model, the precast slab was meshed using an average in-plane element size of approximately 95 mm, with five elements through the 50 mm thickness, ensuring that both flexural behavior and through-depth stress gradients were accurately captured. A finer element size of 25 mm was applied to the concrete surrounding the embedded steel plates and bolt holes to better resolve local stress concentrations. For the connection plates and high-strength bolts, the mesh was further refined to about 10 mm, producing a smooth stress field and improving the stability of the contact iterations. Local mesh refinement zones were also introduced along the steel–concrete interface and the bolt–plate contact regions to enhance the accuracy of contact stress and slip predictions. For the steel truss, the chord members were discretized with an approximate element length of 100 mm along their span.

The nonlinear behavior of concrete was simulated using the Concrete Damaged Plasticity (CDP) model implemented in ABAQUS. The uniaxial stress–strain relationships in tension and compression were defined according to the design code recommendations for C30 concrete, and calibrated using the tested material properties listed in Table 3. The corresponding tensile and compressive damage variables were derived from the post-peak softening branches in tension and compression, respectively, to capture stiffness degradation and crack propagation. For the CDP plasticity parameters, a dilation angle of 30° and a flow eccentricity of 0.10 were adopted, consistent with common practice for normal-strength concrete. The ratio of the biaxial to uniaxial compressive strength was taken as , and the shape factor of the yield surface in the deviatoric plane was set to . A small viscosity parameter of 0.005 was introduced to improve convergence while maintaining quasi-static response.

In the numerical model, point-to-surface contact was defined between the lower steel truss and the connection plate to represent their mechanical interaction. The interaction between the installation bolts and the embedded sleeves was simplified using a bonded constraint, which effectively ensured force transfer between the truss and the precast concrete slab through the bolts. Consequently, the lower truss and the upper slab shared the applied load via the bolted connection, enabling combined load transfer between the two components. Normal contact between the connection plate and the concrete slab, between the connection plate and the installation bolts, and between the precast slab and the rigid support was modeled using a hard contact formulation. The tangential behavior was described using a penalty friction law. A friction coefficient of 0.2 was assigned to concrete–concrete interfaces, while 0.3 was adopted for steel–concrete interfaces (Guo et al. 2023). The rigid support beneath the slab was fully constrained in all degrees of freedom to prevent translation and rotation.

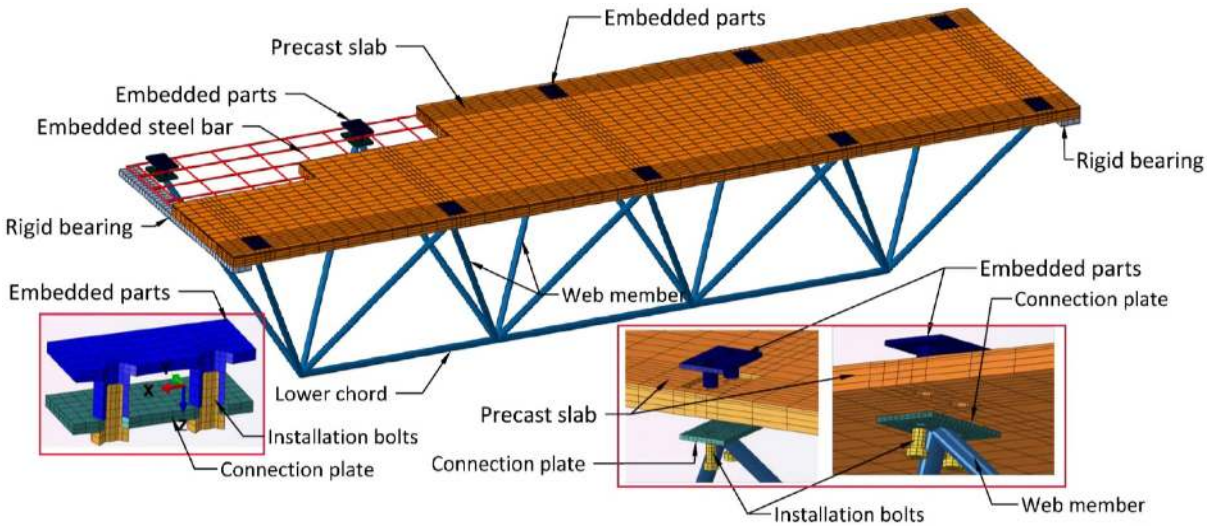

Figure 13 Finite element model schematic diagram.

4.3 Verification of FE model and test results

As illustrated in Figure 14, the monitored vertical displacements for all three specimens rose progressively with the loading steps, peaking at Step 7 (10.0 kN/m^2), and recovered substantially upon unloading. The experimental measurements (EM) and the finite element results (FEM) are consistent in both trend and relative levels: DTs-3 at midspan exhibits the largest displacement, whereas DTs-1 near the support is smaller, which conforms to the deformation pattern of flexural members. For illustration, at DTs-3 in Model 3 (EM-3), the peak displacement measured in the test is 3.75 mm,

whereas the finite-element prediction is 3.07 mm, with the FEA value being smaller by 0.68 mm (18%); After complete unloading, the residual displacements are 0.96 mm (EM) and 0.57 mm (FEM), corresponding to residual ratios of 25.6% and 18.6%, respectively. Overall, the finite element model captures the general deformation trends reasonably well; however, the predicted responses are lower than the experimentally measured values. This discrepancy likely arises from the idealized contact assumptions adopted in the model, which do not fully represent interface slip or the progressive degradation of structural stiffness.

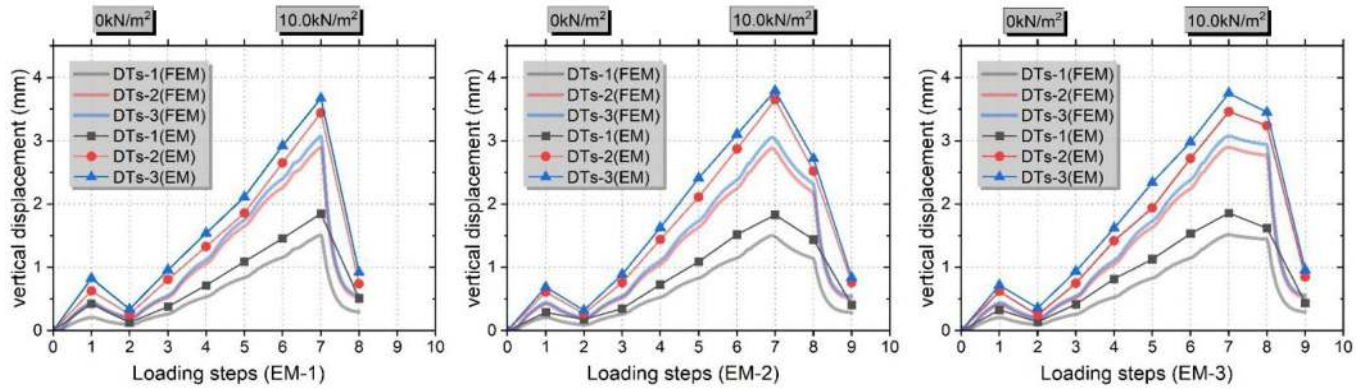

Figure 14 Comparisons of vertical displacement.

As shown in Figures 15–17, the vertical displacements at the three critical monitoring points increase progressively with each loading step, reaching their maximum at step 7 (10.0 kN/m²), and subsequently decrease during unloading. The experimental measurements (EM) and finite element analysis (FEA) results exhibit generally consistent trends and comparable magnitudes. This agreement indicates that the adopted modeling assumptions—including geometric representation, material parameters, and loading procedures—are broadly reasonable, while acknowledging that the numerical model is inherently approximate and cannot fully reproduce the experimentally observed behavior.

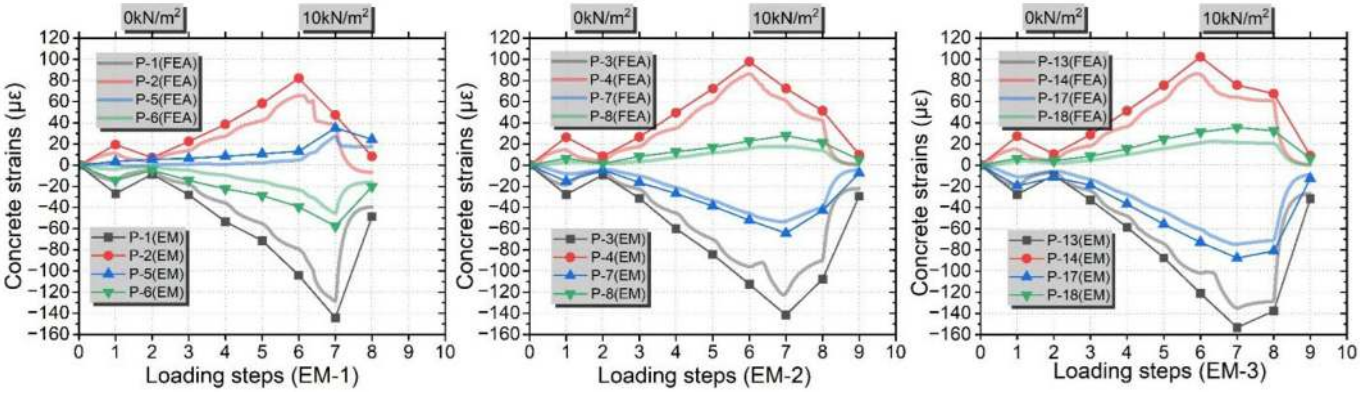

Figure 15 Comparisons of concrete strains.

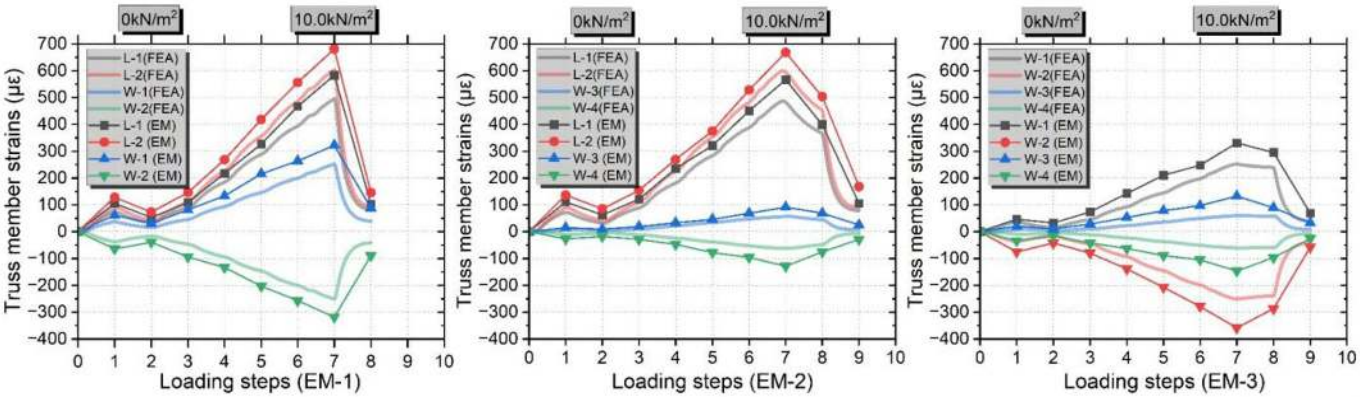

Figure 16 Comparisons of truss member strains.

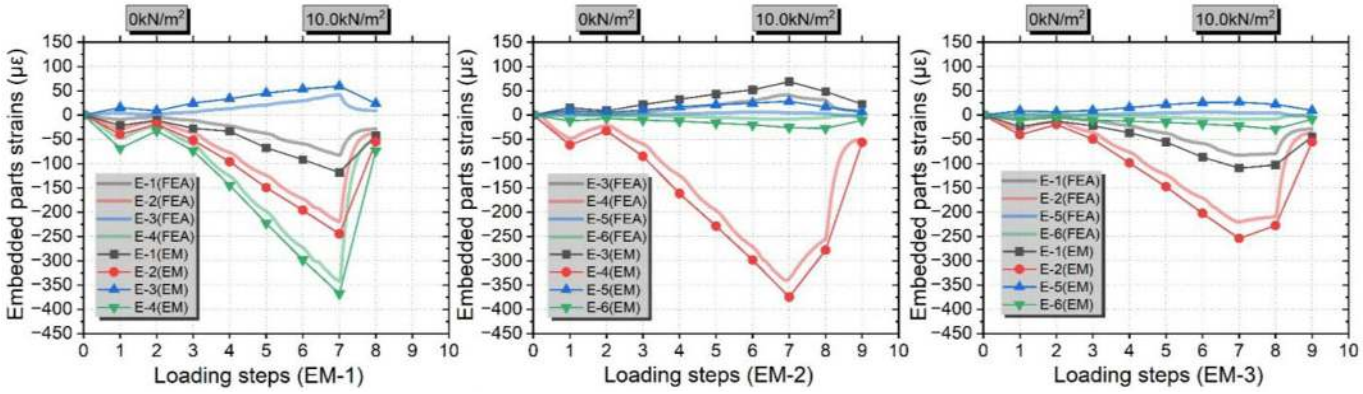

Figure 17 Comparisons of embedded parts strains.

Comparing peak and residual strains, the concrete slab records a peak strain of 153.23 (EM) versus 134.47 (FEA), corresponding to a 12.2% relative error. The residual strains at the same location are 31.55 (EM) and 26.8 (FEA), yielding a 15% relative error. For the truss member, the measured peak strain is 681.15 , compared with an FEA prediction of 602.42 , with a relative error of 11.5%. At the same location, the residual strains are 145.28 (EM) and 88.43 (FEA), corresponding to a 39.1% relative error. For the node plate, the peak strain measured in the test is 374.62 versus 340.15 from FEA, giving a 9.2% relative error. The corresponding residual strains are 56.31 (EM) and 50.09 (FEA), respectively, with a relative error of 11.04%.

The finite element predictions are generally lower than the experimental measurements, suggesting that the actual structure undergoes appreciable plastic deformation during loading. In particular, the connection region between the concrete slab and the embedded plate may experience microcracking, material nonlinearities, and interface slip—complex behaviors that are not fully represented in the present finite element model. Overall, the model provides a qualitatively reliable depiction of the structural response, capturing the general stress–strain evolution and load-bearing characteristics. Nonetheless, the numerical results should be interpreted as approximations rather than definitive predictions.

4.4 Results of FE analysis

Finiteelement Model 2 (FEA2) was selected to investigate the deformation and stress response of the prefabricated concrete composite slab–steel truss modular system under various loading steps. The finiteelement analysis elucidated the deformation patterns of the structure, and, considering the characteristics of the composite system, the overall and local loadtransfer mechanisms were systematically summarized.

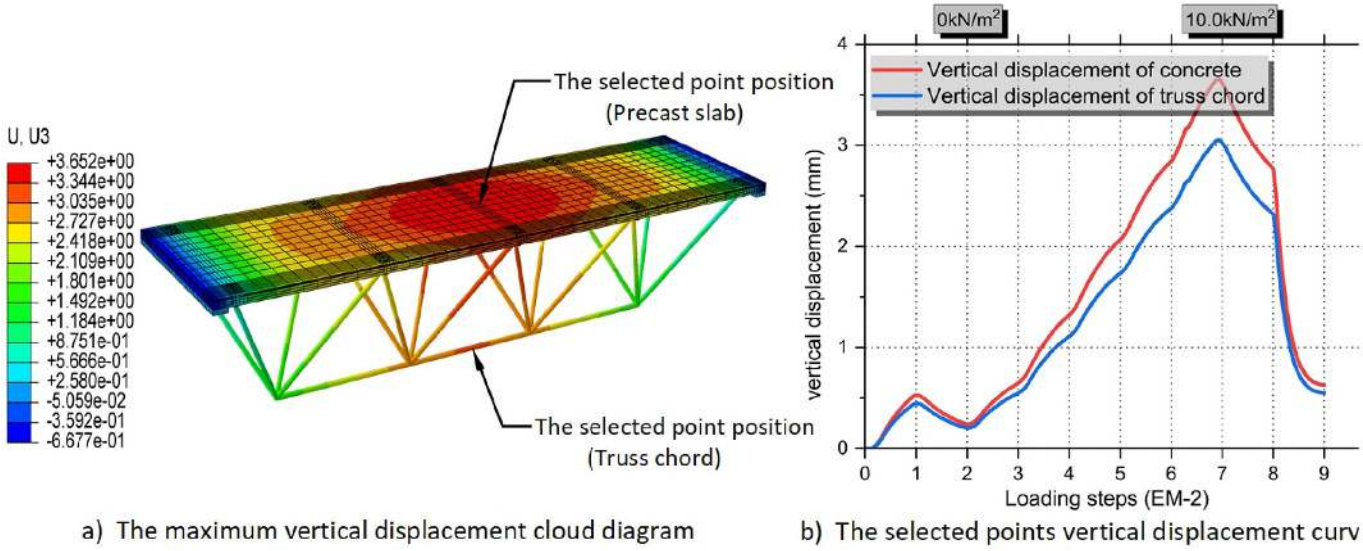

Figure 18 Vertical displacement of FEA model.

The left-hand displacement map in Figure 18 indicates a characteristic bowl-shaped deflection at Step 7 (10.0 kN/m²). The peak vertical displacement of 3.652 mm occurs at midspan and diminishes toward the supports, consistent with the expected behavior of a bending member. The righthand figure presents the displacement histories of the prefabricated composite slab

and the midspan of the lower chord at each loading step. During the initial stages (steps 0-3), the displacements increase gradually; at step 3 the concrete exhibits a vertical displacement of 0.65 mm, while the truss shows 0.55 mm, indicating coordinated deformation between the truss and the concrete slab. In the later loading phase (steps 4-7), the structure enters a stiffnessdegradation regime, and the midspan displacement rises rapidly. At step 7 the concrete vertical displacement reaches 3.65 mm and the truss 3.05 mm, a difference of 16.4 %. During unloading (steps 8-9) the displacements decrease markedly but retain residual values: the concrete retains 0.63 mm and the truss 0.55 mm, corresponding to residual ratios of 17.26 % and 18.0 %, respectively. These results demonstrate a good capacity for deformation recovery. Throughout the entire loading–unloading process, the displacement of the concrete is always greater than that of the truss lower chord, indicating that the two deform in an overall coordinated manner but do not have exactly equal displacements.

Figure 19 presents the distributions of the maximum principal stress on the upper and lower surfaces of the precast composite slab under different loads. When the applied load rises from 2.0 kN/m^2 to 10.0 kN/m^2, the slab's maximum principal stress grows correspondingly, with tension most pronounced on the bottom face. At 10.0 kN/m^2, stresses taper from midspan to the supports, exhibiting the classic bending response of a simply supported member. The transverse constraint imposed by the support attachments and the force transmission at the nodes cause the maximum principal stress to develop initially in the first span adjacent to the support. As the load increases, the tensilestress peak migrates toward the midspan and progressively expands along the length of the span. Due to the support of the lower steel truss and the shear transfer between the embedded plate and the node plate, localized stress concentrations develop in the plate near the nodes, while the stress distribution across the remaining plate area remains relatively uniform. Quantitatively, at a load of 10.0 kN/m^2 the concrete's maximum principal tensile stress is 1.9 MPa, which remains at a relatively low stress level; this is consistent with the experimental observation that no crack development was observed during the test. After unloading is completed, the stresses on both the upper and lower surfaces of the concrete return to their initial levels, indicating that the system has good elastic recovery capacity and limited residual effects.

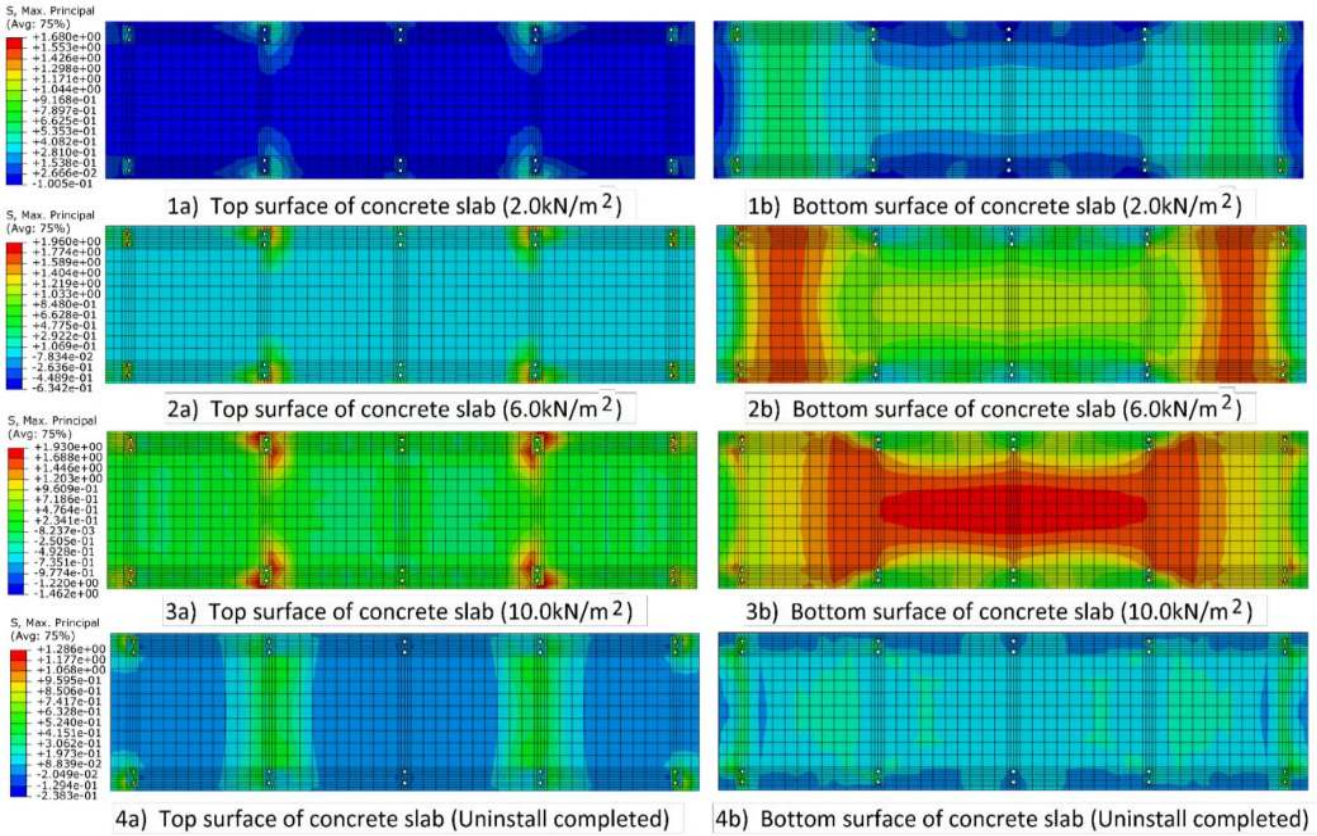

Figure 19 Maximum principal mises distribution of concrete.

Figure 20 illustrates the tensile plastic damage (DAMAGET) and compressive damage (DAMAGEC) obtained from the CDP model under two load levels (6.0 kN/m^2 and 10.0 kN/m^2). At an applied load of 6.0 kN/m^2, the tensile damage is primarily concentrated in the concrete region in contact with the bottom connection plate, while almost no cracking is observed elsewhere in the slab. When the load increases to 10.0 kN/m^2, the tensile damage extends outward from the connection region, yet it remains confined to the vicinity of the joint. Throughout the loading process, compressive damage in the concrete is minimal and can be considered negligible across the entire slab surface. These results indicate

that even under higher load levels, concrete damage remains limited, and the load-transfer mechanism of the detachable joint is not compromised, further confirming the stable structural behavior of the proposed system.

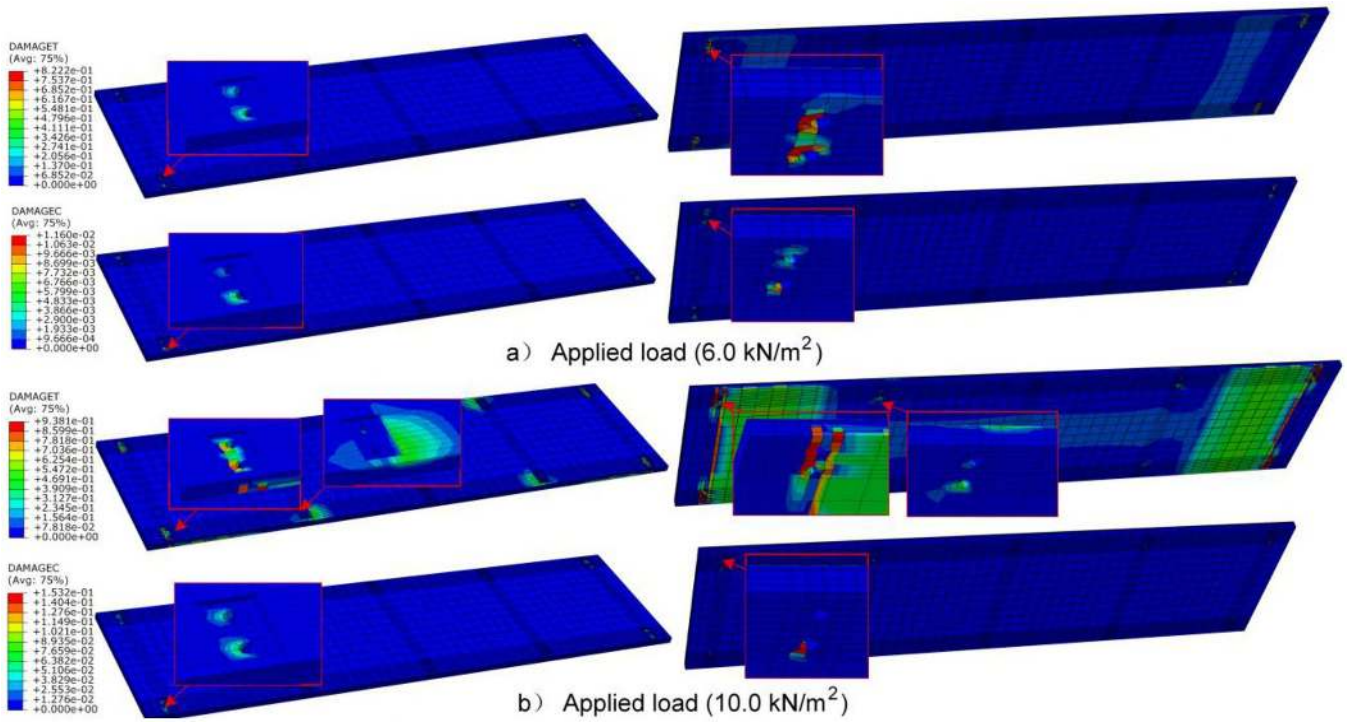

Figure 20 Tensile (DAMAGET) and compressive (DAMAGEC) concrete damage contours.

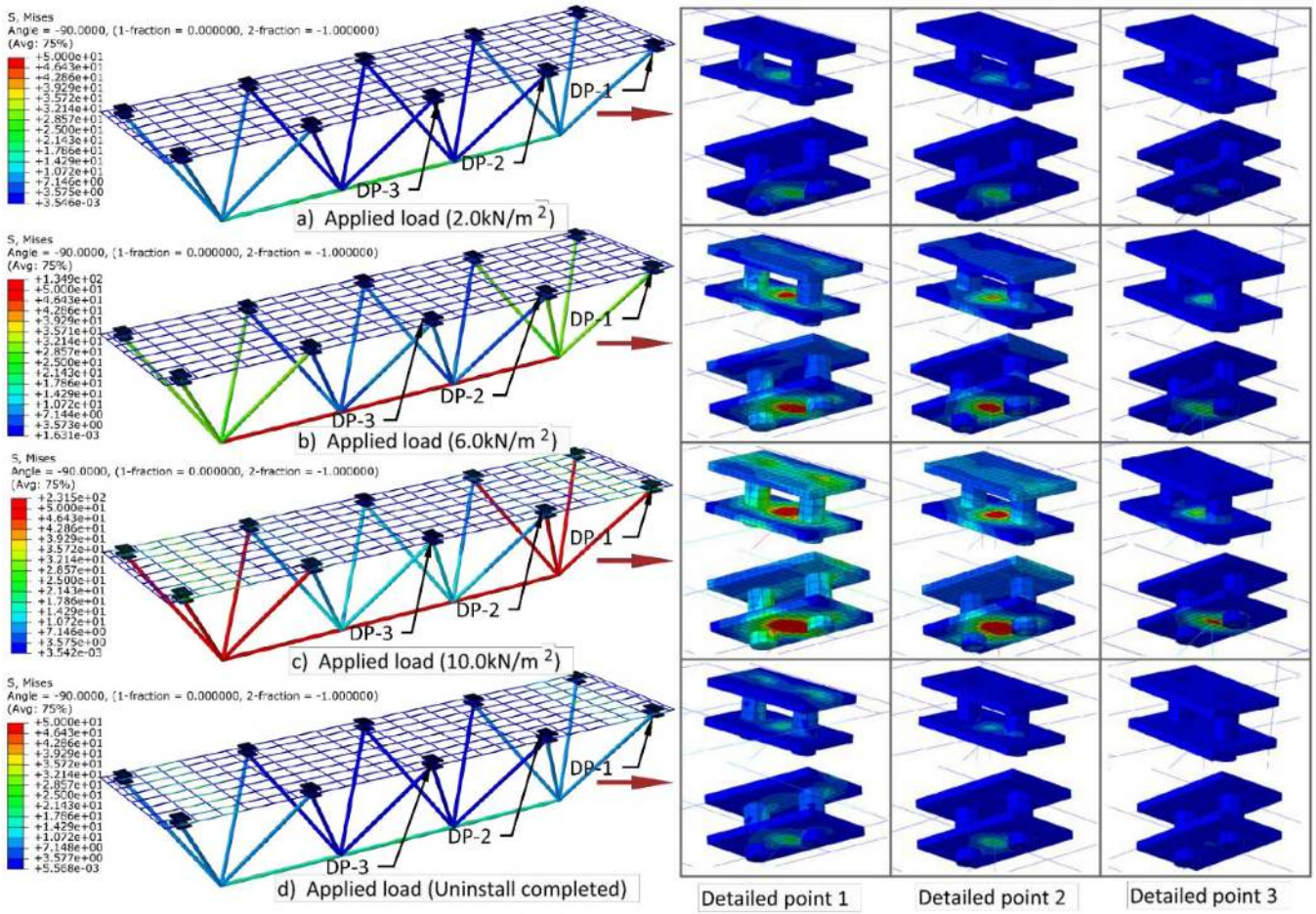

Figure 21 Stress cloud diagram distribution of steel component sections.

Figure 21 presents the von Mises stress distributions of the steel components in the composite structure (reinforcing mesh, truss, and connection joints) under different load levels, and provides enlarged details for three representative joints (DP-1, DP-2, DP-3). As the applied load increases, the stresses in all components rise progressively. The lower chord and the web members near the supports are the primary load-bearing components, and the support restraint produces high-stress zones in nearby webs and connection plates. DP-1 carries higher stress than DP-3, consistent with a response that is shear-controlled near the supports and moment-controlled at midspan. Detail views of the joints indicate that with increasing load, high-stress zones propagate from the lower connection plate upward to the upper embedded plate via the bolts and sleeves (couplers), most prominently at DP-1 adjacent to the support. The stress in the reinforcing mesh within the slab grows relatively steadily with loading; at 10.0 kN/m^2, only the first-span grid near the support exhibits a slight increase, with a stress of about 39.29 MPa, remaining in the elastic range. Following complete unloading, component stresses decrease markedly, and most regions revert to the initial state, indicating that the steel structure as a whole remains predominantly in an elastic state.

4.5 Parameter analysis

To investigate how various parameters affect the mechanical performance of the composite structure, this study conducts a parametric analysis using prefabricated concrete slab thickness, truss member crosssection dimensions, and truss height as the primary variables. The computational model adopts a simplified modeling approach: the concrete slab is modeled with shell elements, the truss portion is modeled with truss elements, and the two are connected at the nodes via tie constraints. With this setup, we derived vertical load–deflection curves at the slab and truss midspan for each parameter set (as illustrated in Figure 22). Compared with the detailed model, the simplified model exhibits some deviation in computational accuracy; however, the overall evolution trend of the loaddeflection curve remains consistent. Consequently, the simplified model can effectively capture the influence of varying parameters on the structural loadbearing performance.

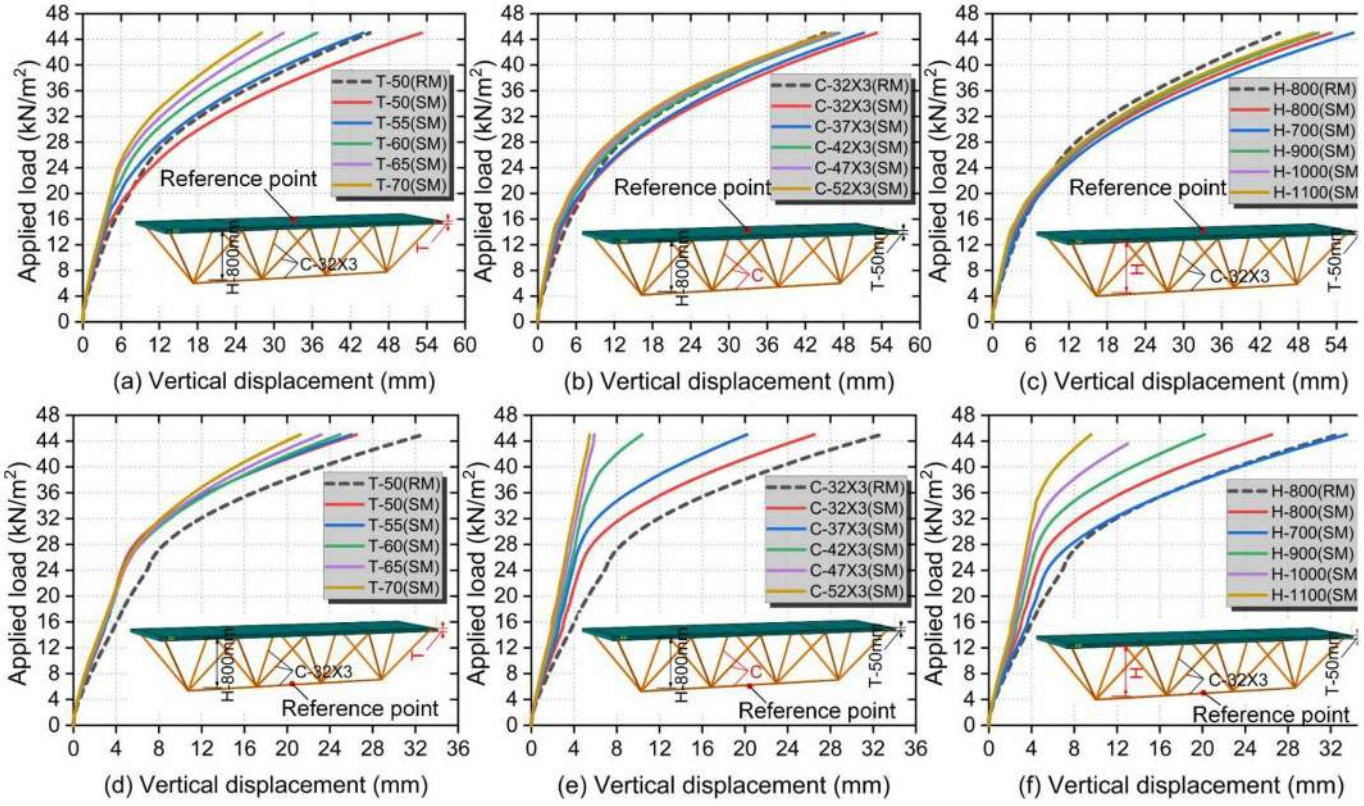

Figure 22 Vertical load-deflection curve under various parameters.

As shown in Figure 22, at a low load level (12 kN/m^2) the load–displacement curves for all parameter configurations nearly overlap, indicating that within the service range the structure responds similarly across parameters. However, as the load increases, the effects of the parameters become pronounced. Figures 22a-22c show that under a loading condition of 45 kN/m^2, increasing the concrete slab thickness from 50 mm to 70 mm reduces the midspan slab deflection by 47.2 %. The wall thickness of the truss members was maintained at 3 mm, while the outer diameter was increased

from 32 mm to 52 mm in 5 mm increments for each analysis case, the slab deflection decreased by 13.4%. In contrast, raising the truss height results in only a 5.8 % reduction in the midspan slab deflection. Figures 23d-e reveal that, under a loading condition of 45 kN/m^2, increasing the concrete slab thickness improves the deflection of the lowertruss span nodes by 19.8 %. In contrast, enlarging the member crosssection and raising the truss height yield substantially greater reductions in deflection, amounting to 79 % and 63.8 % respectively.

Using the inflection point of the truss midspan load–displacement curve to define the system yield, we observe that thickening the slab chiefly benefits the precast slab's own behavior, with diminishing returns as thickness grows, and it does not raise the system-level capacity. By contrast, enlarging truss member sections and increasing truss height markedly enhance the structure's global strength and stiffness.

5 Calculation method for the flexural capacity of structures

5.1 Basic assumption

Tests show that, in the proposed precast slab–steel truss composite formwork system, the lower truss is joined to the upper precast slab through bolts and embedded sleeves. Deformation of these connection nodes induces relative slip between the lower steel truss and the upper concrete panel, which increases the overall deflection of the composite structure and reduces its flexural bearing capacity. Accordingly, the flexural capacity of the prefabricated concrete sandwich panel–steel truss composite formwork is evaluated based on the following assumptions (Nie 1997):

1. The boltedembeddedsleeve connections between the steel truss and the prefabricated concrete panel are assumed to transfer forces effectively, and any slip between the truss and the panel is neglected.
2. The tensile contribution of the concrete panel is ignored, as is the effect of reinforcement embedded within the panel.
3. The influence of the truss web members on the equivalent height of the concretetruss composite system is disregarded.
4. The composite concretetruss structure is assumed to satisfy the planesection hypothesis.

5.2 Calculation of cross-sectional flexural capacity

Given these assumptions, the flexural capacity of the precast slab–steel truss composite formwork system is evaluated under two scenarios, with the corresponding analytical section illustrated in Figure 23.

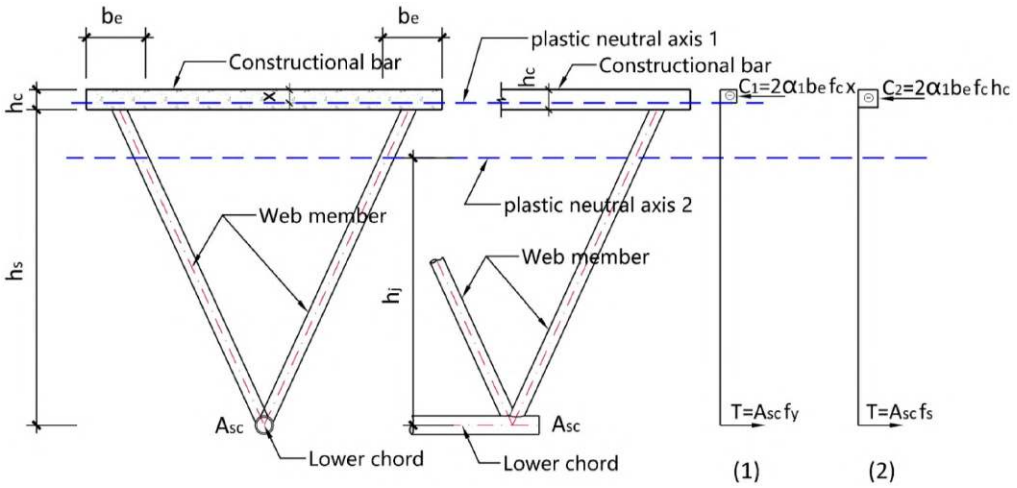

Figure 23 Theoretical model for combined formwork construction with precast concrete laminated slab and steel truss.

(1) Neutral axis within the concrete slab (including the case where it coincides with the lower edge of the slab), , under this condition, enforcing force equilibrium yields:

$$\mathrm{T} = C_1 \tag{1}$$

$$C_1 = 2\alpha_1 b_e f_c x \tag{2}$$

$$\mathrm{T} = A_{sc} f_y \tag{3}$$

The height of the concrete compression zone is given by:

$$x = \frac{A_{sc} f_y}{2\alpha_1 b_e f_c} \tag{4}$$

To ensure that the lower chord of the steel truss yields, the following condition must be satisfied:

$$x \le x_b = \frac{\beta_1 h_c}{1 + \frac{f_y}{0.0033 E_{sc}}} \tag{5}$$

At this stage, the ultimate loadcarrying capacity of the structure can be evaluated using the following expression:

$$M_{u1} = f_y A_{sc} \left(h_s + h_c - x \right) \tag{6}$$

In the above equation: x - height of the concrete compression zone; b_e - twice the distance from the midpoint of the embedded plate to the outer edge of the concrete slab; A_{sc}- crosssectional area of the lowerchord steel tube of the truss; h_c- thickness of the concrete slab; h_s- distance from the centroid of the lowerchord steel tube to the bottom of the concrete slab; f_y- yield strength of the steel; f_c- design compressive strength of the concrete; E_{sc} - elastic modulus of the lowerchord steel tube; α_1 and β_1- calculation factor, whose value is taken from the concrete design code.

(2) When the neutral axis lies within the truss region, $x>h_c$, the entire crosssection of the concrete slab is under compression while the lowerchord steel tube is subjected to tension. In this situation, the lower chord of the truss may either yield or remain below its yield stress; consequently, the sectional capacity is governed by the compressive capacity of the concrete slab. The ultimate flexural resistance of the section can therefore be expressed as follows:

$$M_{u2} = 2\alpha_1 b_e f_c h_c \left(h_s - h_j + 0.5 h_c \right) \tag{7}$$

In the above equation: h_j - The distance from the centroid of the lower chord to the neutral axis.

(3) The foregoing analytical results are predicated on the coordinated action between the concrete slab and the lower truss, assuming that the connection plates linking the lower truss to the embedded concrete panel function properly through bolted joints without any failure. Consequently, an additional verification is required for the case when the bolts reach their critical failure state; under such conditions, the flexural capacity of the section is expressed as follows:

$$M_{u3} = n N_v^b h_s \ge \left(M_{u1}, M_{u2} \right) \tag{8}$$

$$N_v^b = 0.9 n_f \mu P \tag{9}$$

In the above equation: n - calculate the number of bolts in the cross-section; N_v^b - the design shear capacity of a single highstrength bolt; n_f - the number of friction interfaces transmitting load through the bolts; μ - the slip-resistance coefficient of those friction interfaces; P - the pretension force applied to each highstrength bolt.

5.3 Deflection calculation of structures under uniformly distributed load

Prior to deployment, the precast concrete composite slab-steel truss composite formwork system requires verification of its load-bearing capacity and an assessment of serviceability, specifically deflection under applied loading. From the structural mechanics of the system, the overall deflection can be decomposed into two contributing components: (1) The equivalent emptyspan virtual beam undergoes bending deformation. In this representation, the precast concrete slab in the jointed connection region functions as the top chord, while the truss's lower chord serves as the bottom chord. (2) The axial deformation of the web members induces shear deformation in the structure, and it is assumed that the entire shear force is resisted by the web members.

Following the deflection formulation for a simply supported truss–composite beam subjected to full-span uniform loading (Nie 1994), the maximum midspan deflection of the concrete composite slab–steel truss composite formwork system under a uniformly distributed load can be expressed as:

$$f = \frac{5 q L^4}{384 B} \tag{10}$$

In the preceding equation, B - the stiffness of the composite truss accounting for the influence of shear deformation; L - the span of the composite truss.

$$B = \frac{EI}{1+\lambda} \tag{11}$$

In the above expression, EI - the equivalent sectional stiffness of the composite truss, neglecting the contribution of the web members; λ - the stiffness reduction factor associated with the compressive deformation of the web members induced by shear.

$$\lambda = \frac{96I}{5L_w^3} \cdot \frac{(n_l+1)l_w}{A_w \cos^2 \alpha} \tag{12}$$

In the preceding formula, the symbols denote the following quantities, I - the transformed moment of inertia of the composite truss, with the contribution of the web members neglected; A_w - the crosssectional area of the web member, l_w - the length of a web member, n_l - the count of web members over half the span (zero-force members excluded), α - the inclination of the diagonal with respect to the vertical axis.

5.4 The applicability of calculation formulas

To verify the applicability of the theoretical formulas for the loadbearing capacity and deflection of the precast concrete slab-steel truss composite formwork system, the results obtained from the preceding parametric finiteelement simulations are compared with the corresponding theoretical predictions.

Taking EM-2 as an example, the structural load-carrying capacity and deflection were calculated using the proposed theoretical formulas.

The parameters used in the load-carrying capacity calculation are as follows: A_{sc}=273.18 mm^2, b_e =200 mm, h_c =800 mm, h_s=50 mm, f_y =210 N/mm^2, f_c=14.3 N/mm^2 , E_{sc}=2.0X10^5 N/mm^2 , α_1 =1.0, β_1 =0.8;

$$x = \frac{A_{sc}f_y}{2\alpha_1 b_e f_c} = \frac{273.18 \times 210}{2 \times 1.0 \times 200 \times 14.3} = 5.01\ mm\ ;$$

$$x \le x_b = \frac{\beta_1 h_c}{1 + \frac{f_y}{0.0033E_{sc}}} = \frac{0.8 \times 50}{1 + \frac{210}{0.0033 \times 200000}} = 30.35\ mm\ ;$$

$$M_{u1} = f_y A_{sc}(h_s + h_c - x) = 210 \times 273.18 \times (800 + 50 - 5) = 48.47\ kN \cdot m\ ;$$

For evaluating the load-carrying capacity upon bolt failure, the parameters are taken as follows: n=4, n_f=1, μ=0.3, P=155 kN;

$$N_v^b = 0.9 n_f \mu P = 0.9 \times 1 \times 0.3 \times 155 = 41.85\ kN\ ;$$

$$M_{u3} = nN_v^b h_s = 4 \times 41.85 \times 800 = 133kN > M_{u1}\ ;$$

In summary, the calculated load-carrying capacity for specimen EM-2 is 48.47 $kN \cdot m$.

For the deflection calculation of the structure under uniformly distributed load, the parameters are taken as follows: A_w=273.18 mm^2, l_w =964 mm, n_l =8, α = 33.9°, E_c =3.0 X10^4 N/mm^2, q=28 kN/m^2;

equivalent area of a concrete slab:

$$A = \frac{b_c h_s E_c}{E_{sc}} = \frac{1200 \times 50 \times 30000}{200000} = 9000\ mm^2\ ;$$

A concrete section of 1200 mm 50 mm is equivalent to a steel section of 180 mm 50 mm. Neglecting the stiffness of the web members, the transformed upper concrete section and the lower chord yield the combined moment of inertia as follows: $I = 2.323 \times 10^8\ mm^4$;

$$\lambda = \frac{96I}{5L^3} \cdot \frac{(n_l+1)l_w}{A_w\, cos^2\, \alpha} = \frac{96 \times 2.323 \times 10^8}{5 \times 4300^3} \times \frac{(8+1) \times 964}{273.18 \times cos^2\, 3\,3.9^\circ} = 2.586;$$

$$f = \frac{5qL^4}{384B} = \frac{5qL^4\ (1+\lambda)}{384EI} = \frac{5 \times 28 \times 4300^4(1+2.586)}{384 \times 200000 \times 2.323 \times 10^8} = 9.62mm\ .$$

Figure 24 shows that, neglecting interface slip, the proposed theoretical model captures the parametric effects on both strength and deflection, and its predictions follow the same trends as the finite element (FE) results.

Quantitatively, the theoretical ultimate capacity is approximately 60% of the FE estimate, while the FE midspan deflection is roughly 35% of the theoretical prediction. Accordingly, the closed-form approach yields conservative estimates for design. In this structural system, load transfer between the upper precast composite slab and the lower steel truss is achieved through bolted connections. Under higher load levels or complex loading conditions, neither the finite element model nor the theoretical formulas can fully capture the actual load-transfer behavior. Under such conditions, additional experimental data are required to validate the reliability of these formulas before they can be extended to broader applications.

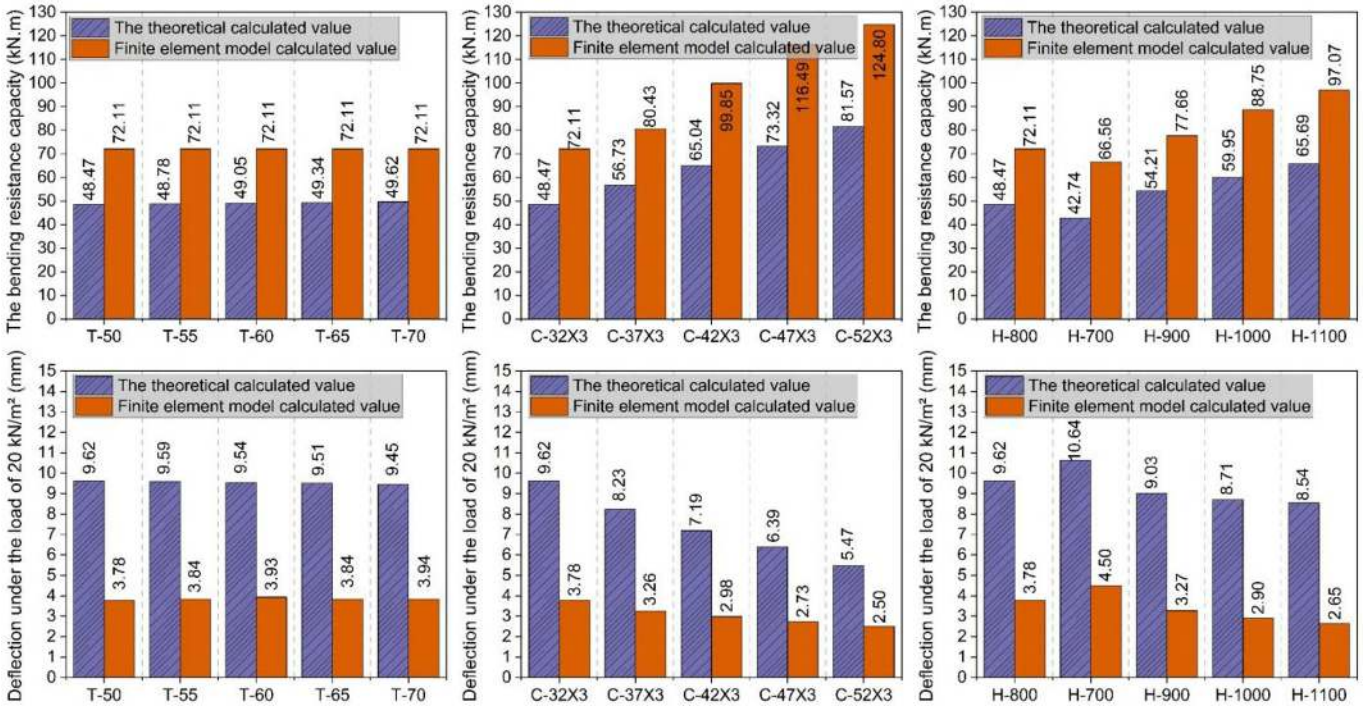

Figure 24 The comparison between the finite element method and theoretical values

5.5 Recommended design parameters for engineering use

Based on the experimental observations, finite-element analyses, and theoretical calculations, the recommended design parameter ranges and corresponding safety considerations for practical engineering application have been summarized in the Paper. The precast concrete composite slab-steel truss composite formwork structural system is suitable for construction-stage slab spans of 3–6 m. For the detachable connections, the installation bolts should be no less than M20 (Grade 10.9) to ensure adequate shear resistance and load-carrying capacity under construction loads, providing an appropriate safety margin.

The precast concrete slab should have a minimum thickness of 60 mm, and the cast-in-place topping layer should also not be less than 60 mm. These requirements help ensure both effective crack control and reliable composite action after hardening. With respect to deformation control, a construction-stage deflection limit of L/800 is recommended, ensuring sufficient stiffness and displacement recovery capability.

The load-carrying capacity and deflection formulas proposed in this study are intentionally conservative, offering an additional margin of safety for design. It should be noted that further refinement and larger-scale experimental validation will be beneficial for broader engineering application in future practice.

6 Conclusion

This paper proposes a precast concrete composite slab-steel truss composite formwork structural system. This study introduces a structural system comprising a precast concrete composite slab integrated with a steel truss composite formwork. Reflecting representative service scenarios, we tested three full-scale specimens through vertical bending load–unload protocols, and complemented the experiments with finite element simulations and parametric analyses. From these efforts, we derive simplified design formulas for predicting ultimate capacity and deflection. Based on the existing results, the following conclusions are obtained:

(1) By incorporating demountable joints, the proposed system enables effective composite action between the upper precast composite slab and the underlying steel truss. This configuration satisfies the unsupported construction requirements of medium and largespan prefabricated decks, markedly improves construction efficiency, and allows the truss to be reclaimed and reused, thereby reducing material consumption. Consequently, the system exhibits strong potential for widespread engineering application.

(2) The full-scale experiments show that global response is governed by flexural deformation, with satisfactory strength performance. Owing to the interaction between the truss and the concrete slab and the force transmission path through the detachable joints, stresses become more concentrated in the web members adjacent to the supports and in the jointplate regions, resulting in a stress distribution that differs from that of conventional purebending members. After unloading, residual deflections are minor, indicating strong recoverability and intrinsic safety redundancy, thereby facilitating component disassembly and reuse. Although the detachable truss system demonstrated stable performance within this study, long-term durability under repeated reuse cycles and environmental corrosion requires further research.

(3) The finite element model developed in this study reproduces the evolution of load bearing capacity and deflection observed in the experiments. The locations and magnitudes of the key monitoring points predicted by the model match the measured values, with errors falling within an engineering acceptable range. These results substantiate the model's suitability for subsequent parametric studies and for design-assessment purposes.

(4) Parametric analyses show that increasing the thickness of the precast composite slab chiefly benefits the slab's local behavior and yields only modest gains in global stiffness and strength. By contrast, enlarging the member cross-sections and increasing the truss height markedly enhance both system stiffness and load-carrying capacity.

(5) The practical calculation methods for load-carrying capacity and deflection proposed in this study reflect the influence of key parameters on the structural response. Within the scope of the present tests and parameter ranges, the calculated results are conservative and may provide a useful reference for preliminary engineering design and scheme evaluation. Nevertheless, additional experimental data are required to further validate the reliability of these formulas before they can be applied to a broader range of structural configurations.

It should be noted that the loading protocol in this study did not consider construction-related dynamic effects, such as vibrations induced during concrete placement and compaction. Future research will further examine the system's response under dynamic loading conditions to ensure that the proposed structural form performs reliably under real construction scenarios.

Acknowledgements

This research is supported by Guizhou University Survey and Design Foundation [Grant No. 202204]; Guizhou Science and Technology Achievement Transformation Foundation [Grant No QKH2023081]; Foundation of Guizhou University GZUF202034; Guizhou University Survey and Design Foundation [Grant No. 202206]; Guizhou Provincial Science and Technology Program Project (Qian Kehe Platform ZSYS [2025] 009).

Author's Contributions: Conceptualization, Tao liang and Jing Chen; Methodology, Tao Liang and Jing Chen; Investigation, Mei Feng; Writing - review & editing, Jing Chen; Funding acquisition, Tao Liang and Jing Chen; Experiment, Yanhui Wei and Hanmin Zhang; Data curation, Mei Feng and Yanhui Wei. All authors have read and agreed to the published version of the manuscript.

Data availability statement: Research data is only available upon request.

Editor: Pablo Andrés Muñoz Rojas

References

Abas F.M., Gilbert R.I., Foster S.J., Bradford M.A., (2013). Strength and serviceability of continuous composite slabs with deep trapezoidal steel decking and steel fibre reinforced concrete. Engineering Structures 49: 866-875.

Araújo D. D., Sales M. W. R., Silva R. P. M., Antunes C. D. M., Ferreira M. D., (2020). Shear strength of prestressed 160 mm deep hollow core slabs. Engineering Structures 218:110723.

B. Y. Deng, D. Tan, L. Z. Li, Z. Zhang, Z. W. Cai, K. Q. Yu, (2023). Flexural behavior of precast ultra-lightweight ECC-concrete composite slab with lattice girders. Engineering Structures 279.

Baran E., (2015). Effects of Cast-In-Place Concrete Topping on Flexural Response of Precast Concrete Hollow-Core Slabs. Engineering Structures 98: 109-117.

GB50010-2010. (2015). Code for Design of Concrete Structures (GB50010-2010). China Construction Industry Press: Beijing, China.

Girhammar U. A., Pajari M., (2008). Tests and Analysis on Shear Strength of Composite Slabs of Hollow Core Units and Concrete Topping. Construction and Building Materials 22: 1708-1722.

Guo Y., Ma K. J., Liu Z. Q., Yu F., Fang Q., (2023). Experimental and numerical investigation of the prefabricated steel–concrete open-web composite floor with embedded chords. Journal of Constructional Steel Research 208:107995.

Hillebrand M., Schmidt M., Wieneke K., Classen M., Hegger J., (2021). Investigations on Interface Shear Fatigue of Semi-Precast Slabs with Lattice Girders. Applied Sciences-Basel 11(23): 11196.

INDUSTRY HANDBOOK COMMITTEE, (2004). PCI Design Handbook: Precast and Prestressed Concrete:6th Edition. PCI. Chicago, IL, USA.

J. G. Nie, J. S. Fan, (2006). The development and prospect of generalized composite structures. Journal of Building Structures 6: 1-8.

JGJ 1-2014. (2016). Technical Specification for Precast Concrete Structure (JGJ 1-2014). China Construction Industry Press: Beijing, China.

Joseph J. D. R., Prabakar J., Alagusundaramoorthy P., (2017). Precast Concrete Sandwich One-Way Slabs Under Flexural Loading. Engineering Structures 138: 447-457.

L. V. Jing, Zhou T. H., Wu H. H., Sang L. R., He Z. Q., Li G., Li K.K., (2020). A New Composite Slab Using Crushed Waste Tires as Fine Aggregate in Self-Compacting Lightweight Aggregate Concrete. Materials 13(11).

Lee K. T., Yang J. M., Kim J. K., (2024). Evaluation of the flexural stiffness of a lattice girder composite slab at the construction stage according to the lattice girder shape. Structures 70:107558.

Li M., Sun Z. Z., Zhao W. J., et al, (2012). Research Progress on Reinforced Concrete Laminated Slab in China. Applied Mechanics and Materials 174(177): 263-267.

Li X., Zhang C. T., An R. B., Zhu H. J., (2025). Flexural behavior of a new type of hollow concrete composite slab. Structures 80:109920.

Lu L. F., Ding Y. Z., Guo Y., Hao H.L., Ding S.L., (2022). Flexural performance and design method of the prefabricated RAC composite slab. Structures 38:572–84.

Lu L., Ding Y., Guo Y., Hao H., Ding S, (2022). Flexural performance and design method of the prefabricated RAC composite slab. Structures 38:572–584.

Lu L., Gao M., Guo Y., Wang W., Yan H., Jiang T, (2022). Experiments on flexural behavior of the prefabricated RAC and NWC composite slab. Ain Shams Engineering Journal 13:101789.

Mohamad N., Khalifa H., Samad A. A. A., Mendis P., Goh W. L., (2016). Structural Performance of Recycled Aggregate in CSP Slab Subjected to Flexure Load. Construction and Building Materials 115: 669-680.

Mohammed B. S., (2010). Structural Behavior and m–k Value of Composite Slab Utilizing Concrete Containing Crumb Rubber. Construction and Building Materials 24(7):1214-1221.

Nie J. G., Shen J. M., (1997). The effect of slip on the flexural strength of steel-concrete composite beams and its calculation. China Civil Engineering Journal 30(1):31-36.

Nie J. G., Shen J. M., Ai Y. S., (1997). General formula for the deformation calculation of simply supported steel-concrete composite beams. China Civil Engineering Journal 11(1):21-27.

Sun J. K., Li R. Y. M., Jiao T., Wang S. P., Deng C. X., Zeng L. Y., (2023). Research on the Development and Joint Improvement of Ceramsite Lightweight High-Titanium Heavy Slag Concrete Precast Composite Slab. Buildings 13(1).

T/CECS 715-2020. (2020). Technical Specification for Application of Lattice Girder Slab (T/CECS 715-2020). China Construction Industry Press: Beijing, China.

Thanoon W. A., Yardim Y., Jaafar M. S., Noorzaei J., (2010). Structural Behaviour of Ferrocement–Brick Composite Floor Slab Panel. Construction and Building Materials 24: 2224-2230.

Tomlinson D., Fam A., (2016). Analytical Approach to Flexural Response of Partially Composite Insulated Concrete Sandwich Walls Used for Cladding. Engineering Structures 122: 251-266.

Wang C. Q., Cheng L. X., Wang Z. Y., Qi C. J., Huang D. M., Wei S., (2024). Preparation and properties of high blending phosphogypsum-desulfurization ash-waste soil based functional prefabricated autoclaved aerated concrete slabs. Construction and Building Materials 423:135879.

Wei J. G., Chen B. C., Wang T.L., (2014). Studies of In-Plane Ultimate Loads of the Steel Truss Web-RC Composite Arch. Journal of Bridge Engineers 19(5).

Wieneke K., Classen M., Hegger J., (2017). Fatigue of Semi-precast Slabs with Lattice Girders. Beton- und Stahlbetonbau 112(9):579-588.

Yin G. A., Ding F. X., Wang H. B., Bai Y., Liu, X. M., (2017). Connection Performance in Steel-Concrete Composite Truss Bridge Structures. Journal of Bridge Engineers 22(3): 04016126.

Yong Y., Liu R. Y., Huo X. D., Zhou X. D., Roeder C.W., (2018). Static Experiment on Mechanical Behavior of Innovative Flat Steel PlateConcrete Composite Slabs. International Journal of Steel Structures 18: 473-485.

Yu J., Sneed L. H., Zhai T. W., Li Y., (2024). Study of the shear bond behavior of a hybrid fiber-reinforced concrete (HyFRC) composite slab. Engineering Structures 312:118232.

Yun Y. C., Jiang J. F., Chen P., (2022). Flexural Behavior of Lattice Girder Slabs with Different Connections: Experimental Study. Advances in Civil Engineering 7722668.

Z. Bayasi, H. Kaiser, M. Gonzales, (2001). Composite Slabs with Corrugated SIMCON Deck as Alternative for Corrugated Metal Sheets. Journal of Structural Engineering 127(10): 1198-1205.

Zhang H., Geng Y., Wang Y.Y., Li X.Z., (2022a). Experimental Study and Prediction Model for Bond Behaviour of Steel-Recycled Aggregate Concrete Composite Slabs. Journal of Building Engineering 53: 104585.

Zhang H., Wang Y. Y., Wang Q. H., Geng Y., (2022b). Experimental study and prediction model for non-uniform shrinkage of recycled aggregate concrete in composite slabs. Construction and Building Materials 329:127142.